Acta Pharmaceutica Sinica B 2024;14(11):5008–5025

Chinese Pharmaceutical Association
Institute of Materia Medica, Chinese Academy of Medical Sciences

Acta Pharmaceutica Sinica B

www.elsevier.com/locate/apsb
www.sciencedirect.com

ORIGINAL ARTICLE

Combination of anti-inflammatory therapy and RNA interference by light-inducible hybrid nanomedicine for osteoarthritis treatment

Li Qiao [a,b,d,†], Zhiyao Li [b,†], Bowen Li [b,*], Fu Zhang [b], Zhuo Yao [b], Chongzhi Wu [b], Honglin Tang [a], Qi Pan [b], Peihua Shi [a,d,*], Yuan Ping [a,b,c,*]

[a]*Department of Orthopaedic Surgery, Sir Run Run Shaw Hospital, Zhejiang University, Hangzhou 310016, China*
[b]*College of Pharmaceutical Sciences, Zhejiang University, Hangzhou 310058, China*
[c]*Liangzhu Laboratory, Zhejiang University, Hangzhou 311121, China*
[d]*Key Laboratory of Musculoskeletal System Degeneration and Regeneration Translational Research of Zhejiang Province, Hangzhou 310016, China*

Received 3 April 2024; received in revised form 8 June 2024; accepted 10 June 2024

KEY WORDS

Osteoarthritis;
Gold nanocages;
Poly(β-amino-ester);
Diacerein;
Pain relief;
Photothermal effect;
Phase-change material;
Combinational therapy

Abstract Osteoarthritis (OA) is a type of highly prevalent heterogeneous degenerative disease that leads to joint pain, deformity, the destruction of articular cartilage, and eventual disability. The current treatment strategies for OA often suffer from systemic side effects, poor anti-inflammatory efficacy, and persistent pain. To address these issues, we develop light-inducible nanomedicine that enables the co-delivery of anti-inflammatory drug (diacerein, DIA) and small interfering RNA (siRNA) targeting nerve growth factor (NGF) for pain relief to enhance the therapeutic efficacy of OA. The nanomedicine is based on poly(β-amino-ester)-coated gold nanocages (AuNCs), which is further incorporated with the phase-change material (lauric acid/stearic acid, LA/SA). Following intra-articular (IA) injection *in vivo*, the nanomedicine displays high degree of drug accumulation and retention in the joint lesion of OA mouse models. The photothermal effect, induced by AuNCs, not only promotes DIA and siRNA release, but also upregulates the expression of heat shock protein 70 (HSP-70) to resist the apoptosis of chondrocytes in the inflammatory condition. The internalization of both DIA and siRNA results in strong anti-inflammatory and pain-relieving effects, which greatly contribute to the joint repair of OA mice. This study offers a promising combination strategy for OA treatment.

*Corresponding authors.
E-mail addresses: bowen_li@zju.edu.cn (Bowen Li), peihua_shi@zju.edu.cn (Peihua Shi), pingy@zju.edu.cn (Yuan Ping).
[†]The authors made equal contributions to this work.
Peer review under the responsibility of Chinese Pharmaceutical Association and Institute of Materia Medica, Chinese Academy of Medical Sciences.

https://doi.org/10.1016/j.apsb.2024.06.009

1. Introduction

Osteoarthritis (OA) is a debilitating multifactorial disease that is primarily characterized by joint dysfunction[1]. OA patients usually endure a progressive loss of joint function and mobility, along with chronic pain and severe stiffness. As a result, long-term treatment is often necessary to alleviate pain symptoms, or in some cases, joint replacement surgery is considered to restore joint function[2]. Extensive research has revealed that articular cartilage dyshomeostasis plays an important role in the pathogenesis of OA, and the dyshomeostasis can lead to extracellular matrix (ECM) degradation and chondrocyte apoptosis, ultimately resulting in cartilage destruction[1,3,4]. Based on these findings, the development of various first-line drugs, such as nonsteroidal anti-inflammatory drugs (NSAIDs), is beneficial for pain relief and improvement of joint function. Nevertheless, all these drugs are unable to effectively alleviate the progression of OA and require long-term treatment. In addition, the overdose of these drugs can lead to limited therapeutic effects and severe side effects[5,6]. Recently, solid evidence indicated that the elevated levels of reactive oxygen species (ROS) are mainly responsible for promoting chondrocyte apoptosis and impairing the ECM[7-9]. Consequently, the injured chondrocytes trigger the release of inflammatory cytokines, which contribute to aseptic inflammation and persistent pain, further driving chondrocyte apoptosis and accelerating the progression of OA[10]. Therefore, the development of ROS-reduced anti-inflammatory drugs holds promising potentials for reducing the apoptosis of chondrocytes and improving the progression of OA.

Diacerein (DIA), a derivative of anthraquinone, has demonstrated the ability to effectively inhibit the expression of inflammatory cytokines and reduce ROS accumulation in OA-impaired chondrocytes[11-13], which facilitates the protection of chondrocytes, anti-inflammatory effect, and pain relief. However, the oral administration of DIA is often limited by the insufficient drug concentration in the joint cavity and is associated with systemic side effects, such as gastrointestinal disorders and cutaneous reactions[14,15]. Intra-articular (IA) injection is another effective treatment option for OA, as compared with other treatments like oral medications or physical therapy[16,17]. Thus, IA injection with DIA can avoid the disadvantages of oral administration in OA treatment, offering an effective approach to enhance the therapeutic effects while reducing side effects[18]. For OA, joint pain is one of the most common and distressing symptoms[1,19]. While clinic anti-inflammatory drugs for OA are primarily designed to target the underlying processes contributing to joint degeneration and inflammation, effective pain management is equally critical for helping OA patients maintain their overall well-being and quality of life[19]. Among pain-relieving therapies, short interfering RNA (siRNA) therapy can specifically inhibit the expression of target genes or pathways associated with pain[20,21], offering a promising target to potentially relieve pain and the prolonged duration of action for OA therapy. Due to the over-expression of nerve growth factor (NGF) in OA progression, therapy targeting NGF has demonstrated efficacy as a specific treatment for alleviating pain in OA[22-25]. Based on these findings, the co-delivery of siRNA targeting NGF (siNGF) and DIA represents a promising and safe combinational strategy to achieve both anti-inflammatory and pain-relieving effects in OA treatment. Previous studies have shown that cationic polymer-functionalized gold nanoparticles (AuNPs) were demonstrated as efficient and safe vehicles for intracellular siRNA delivery[26,27]. These AuNPs not only mediated efficient drug delivery, but also possessed high photothermal conversion properties for triggered drug release or photothermal therapy (PTT)[28,29]. Compared with other types of PTT agents, AuNPs possess a unique localized surface plasmon resonance (LSPR) phenomenon and thus have good photothermal properties[30,31]. Moreover, AuNPs also exhibited low cytotoxicity, good drug loading capacity, and easy surface modification, extending their multiple applications in biomedical fields[32,33]. However, the shortcomings of AuNPs, such as short retention time and lack of targeting, have limited their clinical translational applications. With the advancement of chemical synthesis technology, AuNPs can be synthesized in various shapes and sizes with desired properties[34]. Among these AuNPs, gold nanocages (AuNCs) functionalized with cationic polymers are considered highly efficient co-delivery carriers, which can load siRNA due to their cationic nature[35,36] and small molecular drugs by their porous hollow structure[37-39]. In addition, PTT can trigger the overexpression of heat shock protein 70 (HSP-70) expression[40], playing an important role in protecting the structural integrity and function of chondrocytes, which is conducive to the repair of damaged joint tissues[41]. Additionally, the localized thermal effect induced by PTT facilitates enhanced microcirculatory blood flow within the lesioned region, consequently attenuating inflammation and edema, and this process effectively provides “on-demand” analgesia[40]. For IA injection, the cationic polymer of AuNCs can interact with the negatively charged constituents of cartilage through electrostatic interactions[42-44], enhancing drug accumulation and retention between synovial fluid and cartilage tissue. Overall, the cationic polymer-coated AuNCs may act as a multifunctional carrier for the co-delivery of small molecules and siRNA, offering an effective PTT for OA treatment and enhanced drug retention by IA injection.

Herein, we explored the co-delivery of DIA and siNGF by polymer-coated AuNCs for the combinational treatment of OA. As shown in Scheme 1, AuNCs loaded with DIA are first coated with poly(β-amino-ester) (PBAE)[45,46], the cationic feature of which enables the further complexation with siNGF to afford AuDPNs. In the chondrocytes, the released DIA is expected to counteract the inflammatory factor responses and reduce ROS level, while efficient siNGF transfection allows for pain relief by effectively blocking NGF generation. To further enhance drug retention in the joint lesion, AuDPNs are coated with phase-change materials (lauric acid/stearic acid, LA/SA[47]) to generate AuDPNAs, enabling the controlled release of both drugs through the photothermal effect of AuNCs. After the IA injection of AuDPNAs, effective drug retention in the cartilage tissue was observed due to the positive charge of PBAE[48-50] and the blocking effect of LA/SA, whereas the release of DIA and siRNA can be simply controlled by the photothermal

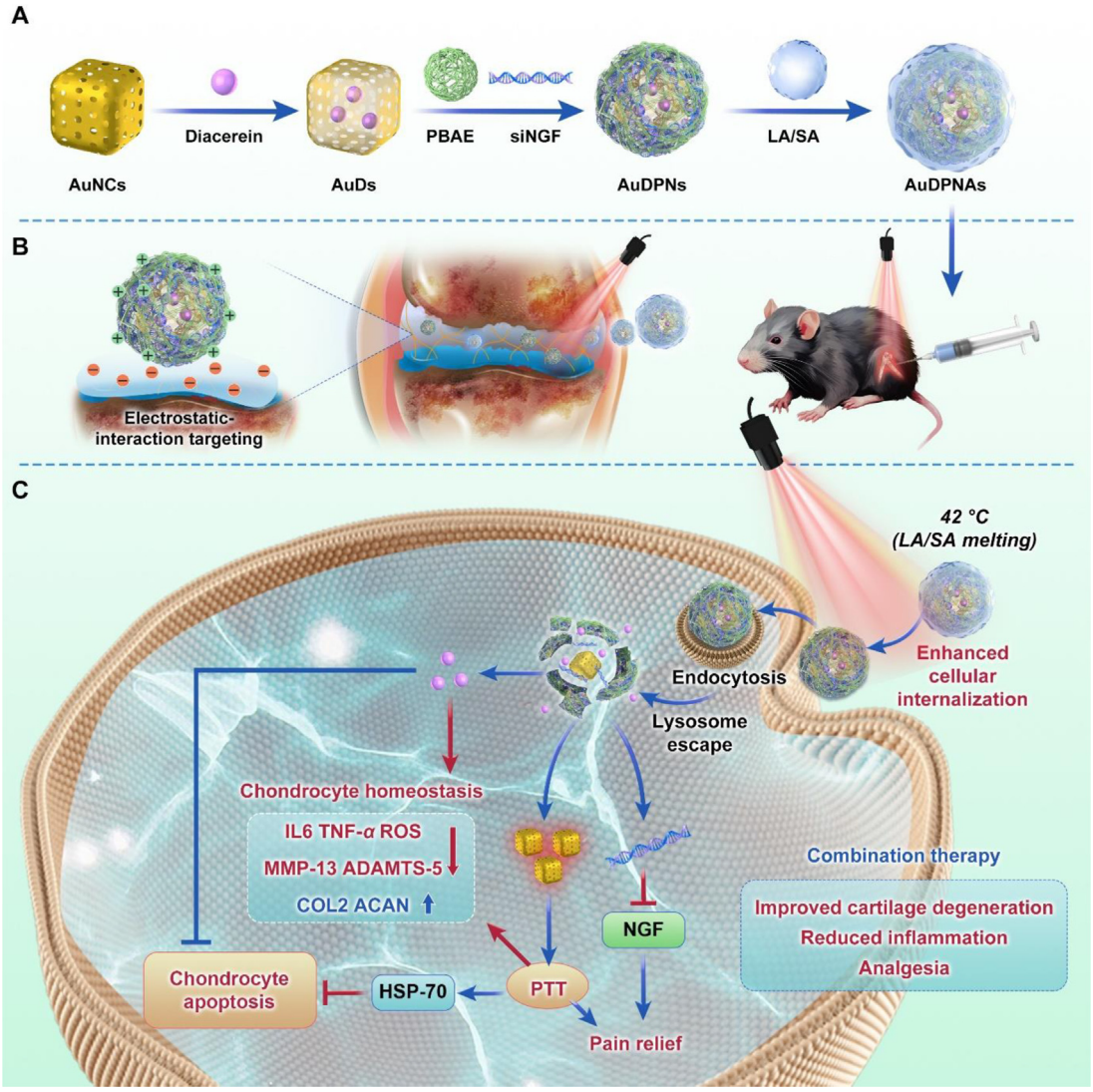

Scheme 1 Schematic illustration of the preparation of AuNCs-based nanodrug system (AuDPNAs) for the co-delivery of DIA and siRNA, and its therapeutic mechanism for OA *in vitro* and *in vivo*. (A) Schematic illustration of the preparation procedures of AuDPNAs nanosystem. (B) The application process and (C) Therapeutic mechanism of photothermally controlled multi-therapeutic nanosystems.

effect. Finally, the strong anti-inflammatory effect, pain relief, recovered joint function and low side effects were clarified in OA mice model. The current study presents a proof-of-concept example of an advanced nanodrug for combinational therapy for precise and safe treatment of OA.

2. Materials and methods

2.1. *Materials*

Chloroauric acid ($HAuCl_4$), Na_2S, poly(vinylpyrrolidone), $AgNO_3$ were purchased from Sigma−Aldrich (Wuxi, China). Diacerein (DIA), Cyanine 5 (Cy5), diacrylate, amine monomers, lauric acid and stearic acid were purchased from Shanghai Aladdin Biochemical Technology Co., Ltd. (Shanghai, China). The NGF siRNA (siNGF) of 5′-GGUUGGAGAUAAGACCACA-3′(1), 5′-CCAUGUUGUUCUACACUCU-3′(2) and 5′-CGACUCACACCU UCGUCAA-3′(3) sequence was purchased from Tsingke Biotech Co., Ltd. (Beijing, China).

2.2. *Instruments*

The ^{1}H nuclear magnetic resonance (^{1}H NMR) spectra were obtained at 500 MHz using a Bruker Avance spectrometer (Bruker, Karlsruhe, Germany). Mass spectra were acquired using the AB Sciex Triple TOF 5600+ LC/mass system (AB Sciex, GA, USA). Measurements for hydrodynamic diameters and zeta potentials were conducted using a Malvern UK Nano-ZS90 dynamic light scattering (abbreviated as DLS; Malvern Panalytical, Shanghai, China). Morphological observations were conducted using a JEM-2010HR transmission electron microscopy (abbreviated as TEM; JEOL, Tokyo, Japan). UV−Vis spectra were captured using a Hitachi U-3010 spectrophotometer (Hitachi, Tokyo, Japan). High-performance liquid chromatography (HPLC) analysis was carried out using an Agilent 1260 m system (Agilent, Beijing, China). Fluorescence images were taken with a fluorescence microscope (IX71, Olympus, Tokyo, Japan). Confocal images were obtained using a confocal laser scanning microscope system (CLSM 880 with fast AiryScan, Zeiss, Jena, Germany).

2.3. Synthesis of AuNCs

We have previously synthesized gold nanorods as photothermal materials, and our efforts showed that these gold nanorods could deliver and activate heat-inducible plasmid DNA[51-53]. In the current study, we synthesized AuNCs by a chemical replacement reaction between chloroauric acid ($HAuCl_4$) and silver nanocubes (AgNCs)[54]. The synthesis of AgNCs followed these steps: Initially, 10 mL of ethylene glycol (EG) was heated to 150 °C using an oil bath while being vigorously stirred. Subsequently, 120 μL of Na_2S solution (3 mmol/L, dissolved in EG) was added to the heated EG solution. After a 4-min mixing period, a 1 mL HCl solution (prepared by mixing 4 μL HCl in 12 mL EG) was added to the mixture and stirred for an additional 2 min. Following this, a poly(-vinylpyrrolidone) solution (2.5 mL, 20 mg/mL in EG, MW ≈ 58,000) was added and stirred for another 2 min. The solution of $AgNO_3$ (50 mg, dissolved in 0.8 mL EG) was then added dropwise and allowed to react for 1 h. The resulting mixture was cooled using ice water and washed with acetone (2 washes of 20 mL each) and water (2 washes of 20 mL each) to yield AgNCs, which were subsequently preserved in water for further applications. To fabricate AuNCs, an appropriate volume of AgNCs was introduced into 10 mL of deionized water (dd water) and heated to 100 °C. Subsequently, $HAuCl_4$ (1 mmol/L, dissolved in water) was slowly added drop by drop. The progression of this reaction was monitored using UV−Vis absorption spectra and stopped upon the emergence of the suitable surface plasmon resonance (SPR) peak at 808 nm. The resultant AuNCs mixture underwent a double rinse with 20 mL each of ethyl alcohol and water before storage in water.

2.4. Synthesis of PBAE

During the formation of cationic PBAE, the diacrylate, backbone amine, and trifunctional amine monomers were amalgamated in a proportion of 1:0.5:0.2. Initially, these monomers were blended in anhydrous dimethylformamide at a concentration of 150 mg/mL. The mixture underwent stirring at 40 °C for 4 h, followed by an escalation to 90 °C for a subsequent 48 h. Upon cooling the amalgamations to 30 °C, an end cap amine was introduced at a 1.5 molar equivalent concerning the excess acrylate and was further stirred for 24 h. The purification process involved a method of dropwise precipitation of the polymers into frigid anhydrous diethyl ether infused with glacial acetic acid. Subsequently, the solution underwent a vertexing process and was centrifuged at 1250×*g* for 2 min to condense into a polymer pellet. The supernatant was then removed, and the polymer was subjected to two additional washes in fresh diethyl ether. Ultimately, it was dried under vacuum for 48 h and stowed at −20 °C.

2.5. Preparation of AuDPNs

A suspension formed by blending 50 mg of AuNCs with 125 mg of DIA (0.06 mmol) in 5 mL of DMSO underwent a 24-h stirring at room temperature in darkness. This mixture was then subjected to centrifugation (12,000 rpm, 10 min; Heraeus Multifuge X1R, Thermo Fisher Scientific, MA, USA) and washed with 20 mL of water twice to remove excess DIA. Afterward, the mixture underwent another 24-h dark stirring at room temperature and was washed twice more (20 mL each) to produce the DIA @AuNCs (AuDs), which was stored at 4 °C. The formation of DIA and siRNA-loaded AuNCs (AuDPNs) engaged the electrostatic interaction between PBAEs and AuDs. Initially, siRNA and PBAEs were combined at N/P ratios of 1:1, 2:1, 3:1, and 4:1 to yield polymeric nanoparticles (siNGF@PBAE). Subsequently, a blend was prepared by suspending 50 mg of AuDs and 10 mg of PNs in 5 mL of DMSO, followed by a 12-h dark stirring at room temperature. This mixture then underwent centrifugation (12,000 rpm, 10 min) and was washed with water twice (20 mL each) to obtain the AuDPNs. To determine the encapsulation efficiency (EE%) and drug loading capacity (LC%) for the nanosystem, the total drug (T_{drug}) was measured and used to obtain nanoparticles (NPs), and then dialyzed with deionized water for 24 h (MWCO = 1000 Da) to measure the free drug (F_{drug}). The EE% and LC% of NPs were detected by UV−Vis spectrometer and calculated according to the following Eqs. (1) and (2):

$$\mathrm{EE}\,(\%) = \frac{T_{drug} - F_{drug}}{T_{drug}} \times 100 \quad (1)$$

$$\mathrm{LC}\,(\%) = \frac{T_{drug} - F_{drug}}{\text{Total weight of NPs}} \times 100 \quad (2)$$

2.6. Preparation of Cy5-loaded gold nanoparticles (AuDs)

The inherent hollow structures within AuNCs facilitated the encapsulation of Cy5. Specifically, 10 mg of Cy5 was integrated with 50 mg of AuNCs in 5 mL of water. After stirring in darkness for 12 h, the mixture was centrifuged (12,000 rpm, 10 min) and washed twice with water (20 mL each) to acquire Cy5-loaded AuNCs (AuDs).

2.7. Preparation of LA/SA-coated nanoparticles (AuDPNAs)

The solution composed of lauric acid and stearic acid (in a 4:1 weight ratio) was initially dissolved in DMSO at a concentration of 4 mg/mL. Then, a 10 mL volume of AuNC-based nanoparticles (AuDPNs) combined with the LA/SA solution (10 μL) was agitated for 3 h at room temperature. The mixture was filtered through a 0.2-μm surfactant-free cellulose acetate membrane. To remove any unencapsulated AuDPNs and DMSO solvents, the Sartorius VIVASPIN 6 centrifugal concentrator (MWCO = 10 kDa; Sartorius, Gottingen, Germany) was used. After three water rinses, the resulting nanoparticles were suspended in water for further applications.

2.8. Electrophoretic gel assay

The Free NGF siRNA (siINGF) and siINGF/PBAEs@AuDs (at *N/P* ratios of 1:1, 2:1, 3:1, and 4:1) were mixed with a loading buffer and applied to a 2% agarose gel. Electrophoresis was performed in 1 × Tris-acetate-EDTA (TAE) buffer at 120 V for 15 min using a JUNYI Electrophoresis Equipment (JY300, Beijing Junyi-Dongfang, Beijing, China). The generated gels were examined under a UV illuminator (FluorChem E System, ProteinSimple, CA, USA), and the RNA bands were detected and imaged with a Gel Documentation System (C150, Azure Biosystems, CA, USA).

2.9. Morphological examination of the nanodrug by transmission electron microscopy (TEM)

The nanoparticles (AgNCs, AuDs, AuDPNs, and AuDPNAs) were formulated in water at a concentration of 1 mg/mL. The

hydrodynamic diameters and Zeta potential of the nanoparticles were gauged using a DLS instrument (Malvern Panalytical). Moreover, a droplet of each suspension was deposited onto a 400-mesh copper grid coated with carbon and left to air-dry. The morphology of the nanoparticles was observed using a TEM (JEOL).

2.10. *In vitro photothermal characteristics of the AuDPNAs*

1.5 mL of AuDPNAs or AuNCs (2 mg/mL, dissolved in PBS) were placed in tubes and exposed to continuous 808 nm light at a power of 0.2 W/cm^2 for 5 min. An infrared light thermometer (FLIR ONE® Pro, FLIR Systems Inc, CA, USA) was used to track temperature variations, while thermal imaging was captured at 1-min intervals. Simultaneously, the temperatures inside the tubes were measured every 30 s. To evaluate photothermal stability, AuDPNAs, prepared at a concentration of 1 mg/mL in PBS, were exposed to 808 nm light at 0.2 W/cm^2 in a cycle of 2 min on and 2 min off, and this process was repeated five times. Temperature readings of the tubes were recorded every 10 s.

2.11. *In vitro DIA release from AuDPNAs*

AuDPNAs were dissolved in the phosphate buffer (pH 7.4) and enclosed within a dialysis bag (Spectra/Por Float-A-Lyzer G2, Cole-Parmer, IL, USA). This bag was then submerged in a centrifuge tube containing 50 mL of the appropriate buffer solution and positioned in a water bath oscillator set at an oscillation speed of 100 rpm. The *in vitro* release assay included different groups exposed or not exposed to laser irradiation. At regular intervals, 4 mL of the solution was extracted from the centrifuge tubes for UV−Vis spectroscopy, and an equal volume of buffer was reinstated into the system.

2.12. *Harvesting and cultivation of chondrocytes*

Chondrocytes were extracted from the knee articular cartilage of neonatal mice through collagenase digestion. The process encompassed cutting the cartilage tissues into 1 mm^3 slices and consecutively treating them. It involved a 0.5 h incubation with 0.25% trypsin (BL512A, Biosharp, Hefei, China) and a subsequent 4 h digestion using 0.2% type II collagenase (BS164, Biosharp, Hefei, China) within a shaking incubator rotating at 90 rpm. The harvested chondrocytes were then cultured in Dulbecco's modified Eagle's medium (DMEM)/F12 media (11320033, Gibco, CA, USA), complemented with 10% fetal bovine serum (A5669801, Gibco, CA, USA) and 1% penicillin-streptomycin solution (BL505A, Biosharp, Hefei, China). Cultivation was conducted within a humidified incubator (BB150-2TCS-L, Thermo Fisher Scientific, MA, USA) at 37 °C with 5% CO_2, and the chondrocytes were maintained within two passages to preserve their cartilage phenotype.

2.13. *Cell viability assay*

DIA, AuDs, siNGF@PBAE, AuDPNs, AuDPNs, AuDPNAs, and AuDPNAs + L were co-cultured with chondrocytes at a density of 10^4 cells per mL in a 96-well plate, at equivalent concentrations of 10 μmol/L for DIA, 0.25 mg/mL for AuNCs, and 1.25 mg/mL for PBAE, respectively. The plate was kept in an incubator set (Thermo Fisher Scientific) at 37 °C with 5% CO_2. Each well was treated with 10 μL of CCK-8 solution (CK04, Dojindo, Kumamoto, Japan), and the cells were then cultured for an additional 2 h and for periods of Days 1, 3, and 5. Afterward, the solution's absorbance was measured at a wavelength of 450 nm using a microplate reader (Infinite F50, Tecan, Mannedorf, Switzerland).

2.14. *Live/dead staining assay*

The chondrocytes were initially cultured and then assessed for viability using a live/dead cell kit (L-3224, life technologies, CA, USA) across different groups. Utilizing a CLSM (Zeiss), cells were treated with 500 μL of live/dead cell dye for 15 min, observed, and subsequently cocultured with DIA, AuDs, siNGF@PBAE, AuDPNs, AuDPNAs, and AuDPNAs + L in triplicate for Days 1, 3, and 5, at equivalent concentrations of 10 μmol/L for DIA, 0.25 mg/mL for AuNCs, and 1.25 mg/mL for PBAE, respectively. As per the manufacturer's instructions, viable cells exhibiting esterase activity emitted a green color, while dead cells with compromised plasma membranes showed a red color.

2.15. *Cell transfection*

The cell internalization behavior of FAM-labeled siNGF (^{FAM}siNGF)@PEI, ^{FAM}siNGF @PBAE, AuDPNs (1:0.5, 1:1, 1:2, 1:3, 1:4, 1:5, 1:6, *w*/*w*) was investigated by CLSM (Zeiss). Chondrocytes were initially seeded in culture dishes at a density of 5×10^4 cells. Following a 24-h incubation, various nanoparticles were added and incubated at 37 °C for an additional 24 h. Subsequently, the medium was aspirated, and the cells were rinsed thrice with PBS. The chondrocytes were treated with 4% formaldehyde and then stained with 4′,6-diamidino-2-phenylindole (DAPI). Fluorescence images were acquired using CLSM.

2.16. *Colocalization assay using Lyso-Tracker Red*

The ^{FAM}siNGF-transfected chondrocytes were co-incubated with Lyso-Tracker Red (C1046, Beyotime Biotechnology, Shanghai, China) at 37 °C for 60, 120, 180, and 240 min, followed by CLSM (Zeiss) analysis. The lysosomes exhibited red fluorescence, whereas ^{FAM}siNGF displayed green fluorescence.

2.17. *Assessment of intracellular reactive oxygen species (ROS)*

Chondrocytes were exposed to DCFH-DA (S0033, Beyotime Biotechnology, Shanghai, China) in fresh culture medium for 20 min and then assessed *via* flow cytometry to determine the DCFH-DA positive rate. Afterward, cells subjected to identical conditions were inspected using a fluorescence microscope (Olympus), and the intracellular fluorescence intensity was measured through flow cytometry.

2.18. *Detection of CAT activity and SOD activity*

SOD activity was assessed utilizing the total superoxide dismutase assay kit with WST-8 (S0101M, Beyotime Biotechnology, Shanghai, China) following the vendor's instructions. DIA, AuDs, siNGF@PBAE, AuDPNs, AuDPNAs, AuDPNAs + L, and SOD enzyme at concentrations of 1, 2, 5, 10, 20, 50, and 100 U/mL were investigated. The WST-8/enzyme working solution (160 μL), initiating solution (20 μL), and sample or control blank (20 μL) were incubated for 30 min at different temperatures (37, 4, or 80 °C). The absorbance was subsequently assessed at 450 nm using a microplate

reader. Similarly, CAT activity of different components was determined using a catalase assay kit (S0051, Beyotime Biotechnology, Shanghai, China). As per the protocol, a 250 mmol/L hydrogen peroxide solution was formulated and standardized using NanoDrop at 240 nm. Subsequently, a mix of 10 μL of the hydrogen peroxide solution (250 mmol/L), either 40 μL for the blank or 35 μL for the catalase standard or sample in the catalase detection buffer, and 5 μL of the catalase standard or sample were blended and left to incubate at 25 °C. After a 2 min incubation period, 10 μL of the reaction solution was blended with 200 μL of color-developing liquid and analyzed using a microplate reader at 520 nm. All results were obtained following the respective assay protocols.

2.19. Cell apoptosis

Cell apoptosis was assessed using the Fluorescein Isothiocyanate (FITC) Annexin V Apoptosis Detection Kit (556507, Becton, Dickinson and Company, NJ, USA) and analyzing the samples *via* flow cytometry. The chondrocytes (2×10^5 cells per well) were initially seeded into a 6-well plate and incubated for 24 h. Afterward, the cells were treated with DIA, AuDs, siNGF@PBAE, AuDPNs, AuDPNAs, or AuDPNAs + L, and further incubated for another 24 h, at equivalent concentrations of 10 μmol/L for DIA, 0.25 mg/mL for AuNCs, and 1.25 mg/mL for PBAE, respectively. The chondrocytes were harvested, rinsed twice with cold PBS, and then stained with Annexin-V-FITC and PI before being analyzed using flow cytometry.

2.20. Quantitative real-time polymerase chain reaction (PCR) analysis

Total RNA was extracted from the chondrocytes following the TRIzol reagent (15596026CN, Invitrogen, CA, USA) protocol that includes critical steps like cell lysis, RNA precipitation, and purification. The extracted RNA, amounting to about one microgram, was then employed to generate complementary DNA (cDNA) using the RevertAid First-Strand cDNA Synthesis Kit (K1621, Thermo Fisher Scientific, MA, USA). This technique comprises RNA priming, reverse transcription of RNA into cDNA, and enzyme inactivation. Subsequently, the synthesized cDNA samples were used for RT-qPCR amplification conducted through the ABI 7500 Sequencing Detection System (7500, Applied Biosystems, CA, USA) and the SYBR Premix Ex Taq Kit (RR420A, TaKaRa, Osaka, Japan). The RT-qPCR process involves several cycles encompassing denaturation, annealing, and extension to measure amplified DNA. Detailed primer sequences used in this study are available in Table 1.

2.21. Enzyme-linked immunosorbent assay (ELISA)

For the evaluation of NGF secretion, supernatants from treated chondrocytes were meticulously collected. Quantitative analysis was then conducted utilizing an ELISA kit specifically designed for NGF detection (BIO-000002, Solarbio, Beijing, China).

2.22. Western blotting

Cell lysates were processed for protein extraction *via* SDS-polyacrylamide gel electrophoresis (ranging from 6% to 12%). The extracted proteins were then transferred onto a polyvinylidene difluoride membrane (0.45 μm). Following a 30 min block with a 5% nonfat dry milk solution in tris-buffered saline with Tween-20, the samples were incubated overnight at 4 °C with various primary antibodies: anti-Bcl2 (ab194583, Abcam, Cambridge, UK), anti-Bax (ab32503, Abcam, Cambridge, UK), anti-Caspase-3 (9662, Cell Signaling Technology, MA, USA), anti-Cleaved Caspase-3 (9661, Cell Signaling Technology, MA, USA), antihSP70 (ab194360, Abcam, Cambridge, UK), anti-ACAN (ab3778, Abcam, Cambridge, UK), anti-COL2A1 (ab34712, Abcam, Cambridge, UK), anti-ADAMT5 (ab41037, Abcam, Cambridge, UK) and anti-MMP13 (ab39012, Abcam, Cambridge, UK). The membranes were subsequently incubated for 1 h with the horseradish peroxidase (HRP)-conjugated secondary antibody (ab205718, Abcam, Cambridge, UK). The protein bands were observed *via* the FDbio-Femto ECL (FD8030, Fudebio, Hangzhou, China) and a chemiluminescence system (ChemiDoc™ Touch Imaging System, Bio-Rad, CA, USA).

2.23. Immunofluorescent staining

The chondrocytes were initially fixed in 4% paraformaldehyde for 20 min and then permeabilized using 0.1% Triton X-100 for an additional 10 min (the COL2A1 assay does not require Triton X-100 treatment). Following this, the cells were incubated in PBS with bovine serum albumin (9048-46-8, Solarbio, Beijing, China) for 30 min. Subsequently, primary mouse ACAN antibodies (ab3778, Abcam, Cambridge, UK), anti-COL2A1 antibody (ab34712, Abcam, Cambridge, UK), anti-ADAMT5 antibody (ab41037, Abcam, Cambridge, UK), and anti-MMP13 antibody (ab39012, Abcam, Cambridge, UK) were applied and left to incubate overnight at 4 °C. Alexa Fluor™ 488-conjugated secondary antibodies (A-11034, Thermo Fisher Scientific, MA, USA) were incubated with the cells for 1 h at room temperature. The cell nucleus was stained with DAPI. Finally, the immunofluorescent images were examined utilizing a CLSM(Zeiss), and software

Table 1 The names of sequences of primers used in this study.

Gene	Primer sequence (forward primer)	Primer sequence (reverse primer)
NGF	5′-CCAGTGAAATTAGGCTCCCTG-3′	5′-CCAGTGAAATTAGGCTCCCTG-3′
COL2A1	5′-CCTGGACCCCGTGGCAGAGA-3′	5′-CAGCCATCTGGGCTGCAAAG-3′
ACAN	5′-AGGATGGCTTCCACCAGTGC-3′	5′-TGCGTAAAAGACCTCACCCTCC-3′
MMP-13	5′-CTTCTTCTTGTTGAGCTGGACTC-3′	5′-CTGTGGAGGTCACTGTAGACT-3′
ADAMTS-5	5′-GGAGCGAGGCCATTTACAAC-3′	5′-CGTAGACAAGGTAGCCCACTTT-3′
TNF-α	5′-CCGTCTCCTACCCGGAAAAG-3′	5′-CGGAATCGGCAAAGTCAAGG-3′
IL-6	5′-TAGTCCTTCCTACCCCAATTTCC-3′	5′-TTGGTCCTTAGCCACTCCTTC-3′

NGF, nerve growth factor; COL2A1, collagen II; ACAN, aggrecan; MMP-13, matrix metalloproteinase 13; ADAMTS-5, a disintegrin and metalloproteinase with thrombospondin motifs 5; TNF-α, tumor necrosis factor-α; IL-6, interleukin-6.

Image J (National Institutes of Health, MD, USA) was employed to determine the mean fluorescence intensity of COL2A1, ACAN, MMP13, and ADAMT-5.

2.24. Animal

C57BL/6 mice (Male, 10-week-old) were purchased from Shanghai SLAC Laboratory Animal Co., Ltd. (Shanghai, China), and the animal handling and experimental procedures were performed with approval from the Institutional Animal Care and Use Committee at Sir Run Run Shaw Hospital, School of Medicine, Zhejiang University, China (approval number: SRRSH202302001).

2.25. Intra-articular (IA) injection and metabolism

Animals used for research were strictly managed in compliance with appropriate laboratory regulations and protocols. Ten-week-old male C57 BL/6 mice were sedated using isoflurane and their limbs were cleaned by three applications of povidone-iodine and 70% (*v*/*v*) ethanol scrubbing. Mice received IA injections of Cy5, AuDs, AuDPNAs, and AuDPNAs + L in the right leg, at equivalent concentrations of 5 mg/kg for Cy5. Radiating efficiency data from each joint was periodically captured over a 28-day period using an IVIS Spectrum imaging system (IVIS Spectrum, PerkinElmer, MA, USA). The distribution of fluorescently labeled formulations was assessed in the knees of mice on Days 0, 1, 3, 7, 14, 21, and 28 post injection.

2.26. In vivo photothermal property of nanodrug

C57BL/6 mice were placed on a platform and subjected to continuous inhalation of 1%−3% isoflurane to induce general anesthesia, the right knee joints of mice were injected with saline, unmodified AuNCs and LA/SA-coated AuNCs (AuDPNAs). The right knees were exposed to 808 nm laser light for 10 min at a power output of 0.2 W/cm^2. Infrared cameras (FLIR Systems Inc) were used to capture thermal images during irradiation, with the laser probe tip 2 cm away from the treated skin for temperature measurement.

2.27. OA mouse model and IA administration

The animal handling and experimental procedures were performed with approval from the Institutional Animal Care and Use Committee at Sir Run Run Shaw Hospital, School of Medicine, Zhejiang University, China. To mimic the chronic osteoarthritis (OA) typically seen in humans, we performed destabilized medial meniscus (DMM) surgery on the right knee of 10-week-old male mice to induce OA. Meanwhile, the control group underwent a sham surgery. Each treatment group received intra-articular injections of the specific composite materials—PBS, DIA, siNGF@PBAE, AuDPNAs, and AuDPNAs + L weekly at DIA content concentrations of 2 mg/kg. In the laser light illumination group, an 808 nm laser light source was used to irradiate the knee joint for 10 min per h, with each treatment cycle lasting 5 h. Additionally, the group exposed to laser light used an 808 nm source to illuminate the knee joint for 10 min per h, creating a 5-h treatment cycle.

2.28. Micro-computed tomography (Micro-CT)

At 4 weeks after the sham/DMM surgery, the mice were humanely euthanized, and the knee joint samples were scanned using a high-resolution micro-CT imaging system (SHIMADZU, Kyoto, Japan).

2.29. Histological and immunohistochemical staining

Knee joint tissues of each group were fixed in 4% formaldehyde for 72 h, followed by decalcification and dehydration. After processing for sectioning, the sections underwent immunohistochemistry (IHC). Following dewaxing and antigen repair, the primary antibodies were applied overnight at 4 °C. Then, the sections were exposed to goat anti-rabbit or anti-mouse IgG HRP (Abcam) for 30 min at 37 °C. The specificity of immunostaining was assessed using an enhanced polymer detection system. Safranin-O/Fast Green staining was performed on the sections to identify cartilage proteoglycan content, and the OARSI scoring system[55-57] gauged cartilage destruction based on this staining.

2.30. OA pain analysis

Pain measurements were conducted using the pressure application measurement (abbreviated as PAM; IITC Life Science Inc., CA, USA) device at 1, 2, and 4 weeks post the sham/DMM surgery. Mice were acclimated to stable environmental conditions for two days before testing. The PAM tests involved applying force to the knee joint until signs of discomfort or pain appeared. The device recorded the peak force within a 5-s duration, displayed in grams as the paw withdrawal threshold.

2.31. Behavioral evaluation

The spontaneous behavior of the mice was monitored using the LABORAS system (Metris, Hoofddorp, Netherlands). Five mice from each group were simultaneously assessed on five platforms over a 15-h period, starting at 6:00 pm and ending at 9:00 am the following day. The parameters evaluated included locomotion distance and average speed.

2.32. Statistical analysis

The data are presented as mean ± standard deviation (S.D.). One-way analysis of variance (ANOVA) was employed for multiple comparison tests. Two-way ANOVA with a Bonferroni *post-hoc* test was employed when two parameters were considered. Statistical significance was denoted as $^*P < 0.05$, $^{**}P < 0.01$, or $^{***}P < 0.001$.

3. Results and discussion

3.1. Preparation and characterization of nanodrug AuDPNAs

The AuDPNAs were synthesized using the top-down approach as shown in Fig. 1A. Firstly, AuNCs were synthesized according to the previous literature[54], and were confirmed by characteristic absorbance peaks at 808 nm (Supporting Information Fig. S1). In addition, the size distribution and morphology of AuNCs, determined by dynamic laser scattering (DLS) and transmission electron microscopy (TEM), revealed that the average hydromechanical diameter was about 51.28 nm with obvious

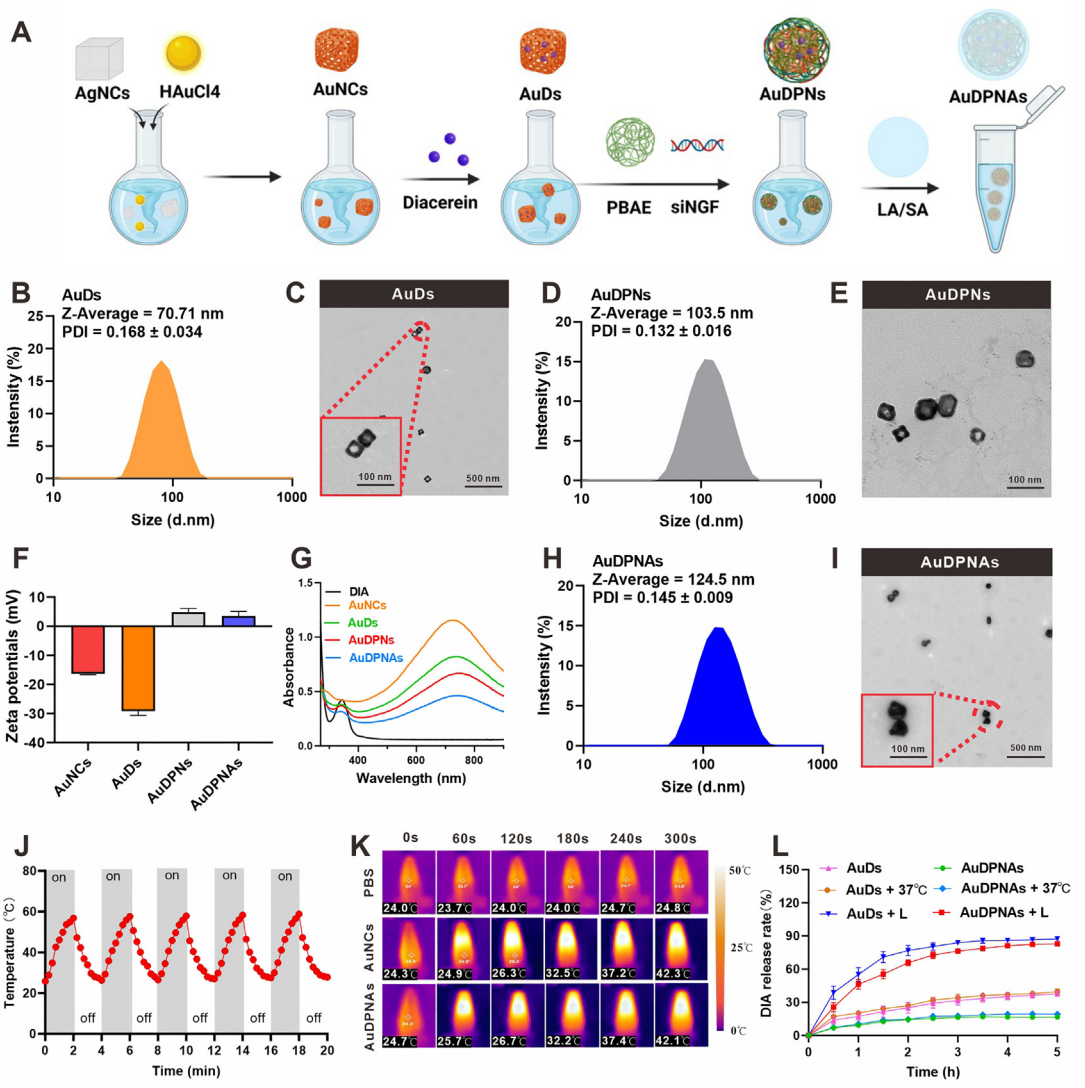

Figure 1 Preparation, characterization, and *in vitro* release behavior of nanodrug. (A) Schematic illustration for the formations of AuDPNAs. (B−E) TEM image and size distribution of AuDs and AuDPNs. Scale bar: 100, 500 nm. (F) The zeta potentials of AuNCs, AuDs, AuDPNs and AuDPNAs were determined by DLS. (G) The absorbance spectra of AuNCs, AuDs, AuDPNs and AuDPNAs were determined by UV−Vis spectrometer. (H) TEM image of AuDPNAs. (I) Size distribution of AuDPNAs. Scale bar: 100, 500 nm. (J) Photothermic stability of AuDPNAs upon 808 nm laser irradiation of 0.2 W/cm^2 for five on/off cycles at room temperature. (K) The laser thermography of PBS, AuNCs and AuDPNAs with 2.0 mg/mL after 808 nm laser irradiation of 0.2 W/cm^2 for 5 min. (L) *In vitro* release profiles of DIA from AuDs and AuDPNAs with or without laser irradiation/37 °C water bath for 5 h determined by UV−Vis.

hollow interiors and pores (Supporting Information Fig. S2). To achieve the co-delivery of siNGF and DIA, DIA was initially encapsulated within AuNCs to form nanocomplex AuDs (Fig. 1B and C). These AuDs were subsequently coated with cationic polymer PBAE, culminating in the formation of AuDPs (Supporting Information Fig. S3). The AuDPs then facilitated the complexation of siRNA by electrostatic interactions, thereby forming AuDPNs. As shown in Fig. 1B and D, the average hydromechanical diameter of AuDs and AuDPNs increased to 70.71 and 103.5 nm, respectively. Moreover, TEM images depicted the cuboidal shape of AuDPNs with a size of around 80 nm, and a fuzzy layer on the AuNCs surface confirmed the successful modification with PBAE (Fig. 1E). The zeta potential shifted from negative (−29.9 mV) to positive (8.5 mV) upon PBAE coating (Fig. 1F). In AuDs and AuDPNs, there were two obvious absorbance peaks (340 nm and 808 nm), which were correlated to DIA and AuNCs, respectively (Fig. 1G). Furthermore, we also calculated the drug-loading capacity (LC%) and encapsulation efficiency (EE%) of AuDs NPs according to the standard calibration curves (Supporting Information Fig. S4). The EE% and LC% of DIA was about 67.4%, and 46.5%, respectively. Finally, the loading efficiency of siNGF on AuDPNs was confirmed by the agarose gel electrophoresis assay, and we found that the migration of siNGF was totally inhibited by PBAE@AuDs when the *N*/*P* ratio reached 3:1 (Supporting Information Fig. S5). The stability of the AuDPNs nanohybrid system was demonstrated by the

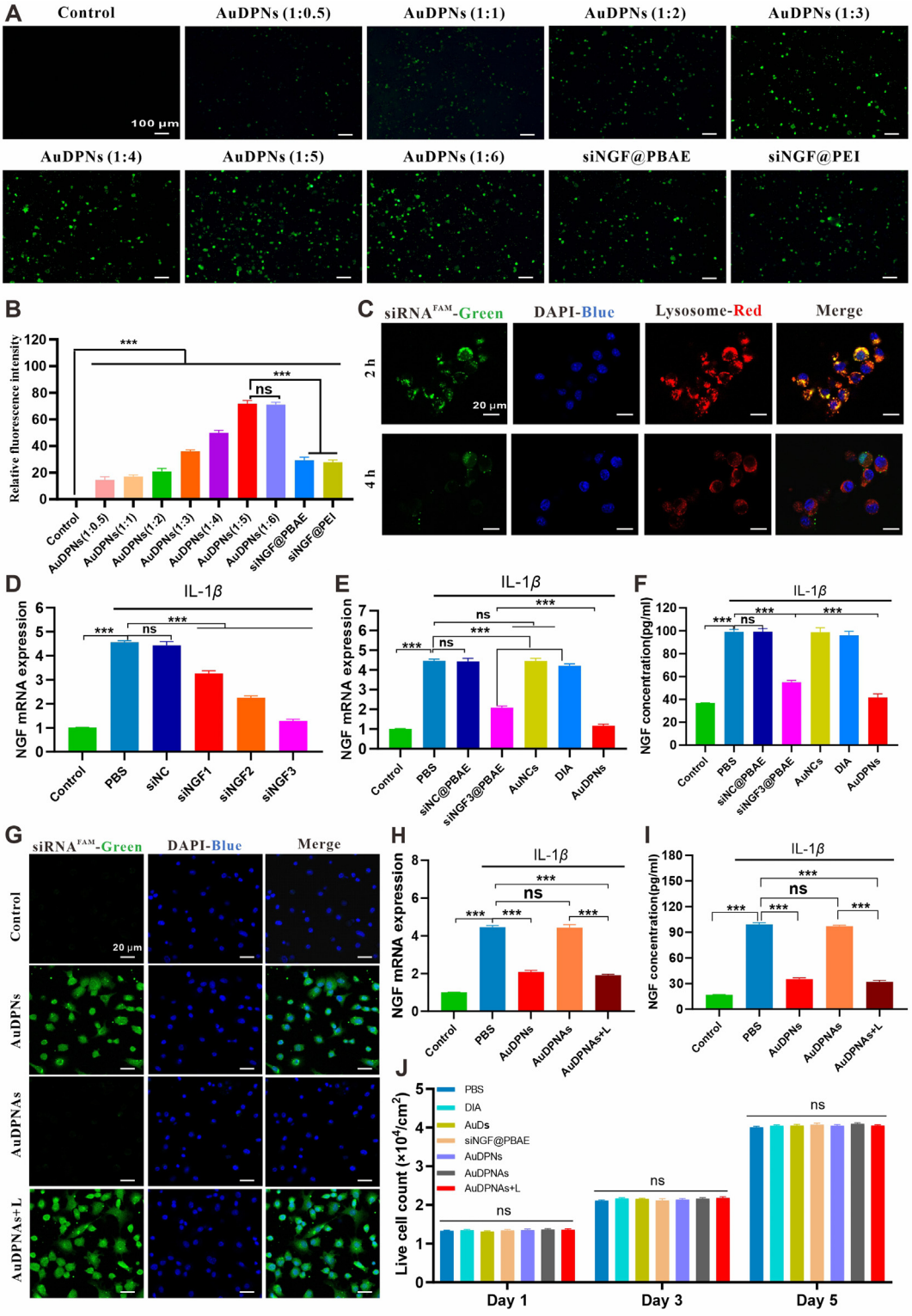

Figure 2 *In vitro* transfection, photothermal-responsiveness and biocompatibility of the nanodrug with chondrocytes. (A) Illustration for fluorescence intensity of the FAM-labeled siRNA in chondrocytes after transfection by siNGF@PEI, siNGF@PBAE, and AuDPNs at various mass ratios of AuNCs/PBAE (1:0.5, 1:1, 1:2, 1:3, 1:4, 1:5, 1:6, *w/w*). Green, siRNA. Scale bar: 100 μm. (B) The fluorescence intensity of chondrocytes was quantitatively assessed by flow cytometry after transfection. ($n = 4$). (C) The cellular uptake and endosomal escape of AuDPNs in chondrocytes were observed *via* confocal laser scanning microscopy (CLSM). Green, siNGF; Blue, nucleus; red, LysoTracker red; yellow, colocalization of siNGF and LysoTracker red. Scale bar: 20 μm. (D) Relative NGF expression of chondrocytes treated with IL-1β (10 ng/mL) at negative control siRNA (siNC) and three siNGFs transfection, respectively ($n = 3$). (E, F) NGF expression (E) and secretion (F) in chondrocytes stimulated with IL-1β and co-treated with PBS, siNC@PBAE, AuNCs, diacerein (DIA) and AuDPNs for 24 h by RT-qPCR and ELISA,

observation of no significant fluctuations in particle size over a 15-day period (Supporting Information Fig. S6). To endow the nanodrug with photothermal-responsive drug release, we utilized a photothermal-responsive phase-transition material (lauric acid/stearic acid, LA/SA) to coat with AuDPNs. The resulting LA/SA-coated nanodrug, AuDPNAs, exhibited a slightly larger size distribution (124.5 nm) (Fig. 1H), as confirmed by less prominent hollow interiors due to the LA/SA coating revealed by TEM (Fig. 1I). Noted that the positive potential and absorbance peak of AuDPNAs were similar to those of AuDPNs (Fig. 1F and G).

3.2. *In vitro photothermal effect and release behavior of AuDPNAs*

To evaluate the photothermal properties of AuDPNAs, the time-dependent temperature changes were measured by the laser irradiation. As shown in Supporting Information Fig. S7, AuDPNAs exhibited excellent photothermal conversion at concentrations ranging from 0.25 to 2.0 mg/mL. In addition, after five repeated heating and cooling cycles, the photothermal maintained a controllable temperature fluctuation with minimal changes, indicating good photothermal stability and high photothermal efficiency (Fig. 1J). In addition, the time-dependent temperature elevation of AuDPNAs was comparable to AuNCs (Fig. 1K). All these results suggested that AuDPNAs exhibited good photothermal properties and photostability. The LA/SA mixture, which was in a solid state at room temperature and can transit into liquid state above 39 °C, was incorporated to impart photothermal responsiveness for controlled drug release[47]. As shown in Fig. 1L, the release rate of DIA increased to 80% under photothermal effect for 5 min, while poor release of DIA from AuDPNAs was observed with or without 37 °C incubation. Moreover, the drug release of DIA obviously increased with the temperature elevation to 42 °C, suggesting that the coating LA/SA can effectively promote the photothermal-responsiveness release of DIA.

3.3. *In vitro transfection, NGF expression and biosafety of AuDPNAs*

To investigate the transfection of PBAE-modified AuNCs, AuDPNs were first complexed with siRNA (labeled with a FAM fluorophore) at different mass ratios of AuNCs/PBAE and were then incubated with chondrocytes. In Fig. 2A, the highest transfection efficiency, as revealed by the strongest fluorescence signal, was observed at the weight ratio of 1:5, which was higher than that of free PBAE and PEI. Moreover, the similar results were confirmed by flow cytometric analysis (Fig. 2B). To assess the endosomal escape of AuDPNs, lysosome and cell nuclei were labeled with red (LysoTracker red) or blue dye (Hoechst 33342), respectively. After 2 h of incubation, the green signal from AuDPNs colocalized with the red signal in the cells, indicating the initial distribution in lysosomes. After 4 h, the green fluorescence already spread out from the red fluorescence of the lysosome, indicating the successful escape of siRNA from the lysosome into the cytoplasm (Fig. 2C). To elucidate the specific internalization pathways, various inhibitors were administered prior to the transfection of chondrocytes (Supporting Information Fig. S8). The intracellular delivery efficiency of AuDPNs was markedly reduced from 53.3% to 15.9% in the presence of methyl-β-cyclodextrin (M-β-CD), a caveolae-dependent endocytosis inhibitor. Meanwhile, the transfection efficiency also decreased by the addition of a proton-pump inhibitor, bafilomycin A1 (BafA1). The combination of M-β-CD and BafA1 could further suppress the delivery efficiency to 4.5%. Moreover, a significant reduction in the uptake of AuDPNs at 4 °C indicates that internalization is energy-dependent. These findings collectively suggest that the internalization of AuDPNs complexes by chondrocytes occurs predominantly through the caveolae-dependent pathway, with subsequent endosomal escape potentially mediated by the proton-sponge effect.

Interleukin-1β (IL-1β), a well-known pro-inflammatory mediator in OA, induces the production of NGF by chondrocytes in cartilage tissue[4,58]. Therefore, IL-1β treatment (10 ng/mL) was chosen to induce NGF expression in chondrocytes, followed by transfection with negative control siRNA (siNC) and three siNGFs, respectively. Quantitative reverse transcription PCR (RT-qPCR) analysis demonstrated a significant increase of NGF mRNA expression in chondrocytes treated with IL-1β or co-incubated with siNC. Conversely, NGF expression was inhibited by different siNGFs, among which siNGF3 exhibited the most significant inhibitory impact (Fig. 2D). Based on these results, siNGF3 was selected as the best candidate for siRNA treatment. The RT-qPCR results clearly indicated that there was no suppression effect on NGF expression in the blank, siNC@PBAE, AuNCs, or DIA groups. AuDPNs were able to knockdown NGF expression in chondrocytes, with both groups exhibiting superior efficacy compared to siNGF3@PBAE (Fig. 2E). Moreover, enzyme-linked immunosorbent assay (ELISA) also revealed the significant knockdown of NGF protein secretion in the AuDPNs groups (Fig. 2F). All these results suggest that AuDPNs were effective in delivering siNGF and generated the robust knockdown of NGF expression.

The phase-change materials LA/SA could transform into a liquid state at a temperature of around 42 °C, and thus low-power laser irradiation was used to elevate the temperature by photothermal effect. Compared with AuDPNs, the cellular uptake of ^{FAM}siRNA greatly decreased in the AuDPNAs group. After irradiation for 3 min, the fluorescence intensity of AuDPNAs was comparable to that of AuDPNs (Fig. 2G and Supporting Information Fig. S9). To further validate the photothermal-responsive siRNA transfection mediated by AuDPNAs, the expression of NGF was investigated using RT-qPCR and ELISA.

respectively ($n = 3$). (G) Distribution of siNGF in chondrocytes after transfection by AuDPNs, AuDPNAs and AuDPNAs + L by a CLSM. Green, siRNA; Blue, nucleus. Scale bar: 20 μm. (H, I) NGF expression (H) and secretion (I) in chondrocytes stimulated by IL-1β, and co-treated with AuDPNs, AuDPNAs and AuDPNAs + L for 24 h ($n = 3$). (J) The quantity of viable cells obtained from the Live/Dead assay of chondrocytes co-cultured with PBS, DIA, AuDs, siNGF@PBAE, AuDPNs, AuDPNAs, and AuDPNAs + L ($n = 3$ biologically independent samples). Data are presented as mean ± S.D. Significance was calculated using one-way ANOVA with Tukey's *post-hoc* test. ***$P < 0.001$. ns, no significant difference.

With the shielding effect of LA/SA, the NGF-silencing effect of AuDPNs experienced substantial inhibition, yet it was subsequently recovered after the laser irradiation (Fig. 2H and I), suggesting the photothermal release of siRNA. Live/Dead staining showed that over the course of a 5-day culture, most of the chondrocytes treated with AuDPNs remained alive. The cell density gradually increased from Day 1 to Day 5 (Supporting Information Fig. S10A), which was also confirmed by the incremental number of viable cells (Fig. 2J). Additionally, the CCK-8 test showed that compared with the control group, there was no significant difference in the proliferation activity and cell viability among the experimental groups at all time points (Fig. S10B). All these results indicated that AuDPNAs exhibited low cytotoxicity to the chondrocytes.

3.4. *In vitro therapeutic effect of AuDPNAs*

In the pathogenesis of OA, inflammation and oxidative stress are closely associated with the disease progression. The local inflammatory response within the joint is accompanied by cartilage degeneration, leading to the increased oxidative stress response and apoptosis in chondrocytes. Oxidative stress and chondrocyte apoptosis further exacerbate the imbalance of cartilage metabolism, forming a vicious cycle that aggravates OA development[7,8,10]. Many previous works have demonstrated that IL-1β could induce chondrocytes to generate oxidative stress and pro-inflammatory effects[59,60]. To mimic the *in vitro* pathological condition of OA, the chondrocytes were first treated with IL-1β (10 ng/mL) and then the therapeutic effect of AuDPNAs + L was evaluated. Elevated ROS level was an important indicator of oxidative stress, and we first investigated the ROS level of chondrocytes by 2',7'-dichlorodihydrofluorescein diacetate (DCFH-DA) fluorescent probe. After pretreatment with IL-1β, an obvious fluorescence signal of PBS and siNGF@PBAE was observed, while the free anti-inflammatory drug, DIA, exhibited a poor fluorescence signal under the same conditions, suggesting the inhibition of ROS generation (Fig. 3A). Moreover, AuDs and AuDPNs also displayed good ROS inhibition due to the release of DIA from these two groups. Similarly, laser irradiation could trigger DIA release from AuDPNAs to inhibit ROS generation, which was also confirmed by flow cytometry results (Supporting Information Fig. S11). In addition, two important antioxidant enzymes, namely superoxide dismutase (SOD) and catalase (CAT)[8], were also investigated in chondrocytes. As shown in Fig. 3B and C, nanoparticles containing DIA (AuDs, AuDPNs, and AuDPNAs + L) all effectively improved the activities of SOD and CAT, as opposed to free DIA which is difficult to diffuse into cells. All these results proved that AuDPNAs + L treatment could effectively release DIA and exhibited strong ability to inhibit ROS generation.

The loss of chondrocyte vitality is a notable characteristic of OA, and chondrocyte apoptosis is another key indicator of the procession of cartilage degeneration[61]. Thus, IL-1β-induced apoptotic progression of chondrocytes was determined by flow cytometry using annexin V−FITC assays. As shown in Fig. 3D and Supporting Information Fig. S12, DIA, AuDs, and AuDPNs obviously alleviated chondrocyte apoptosis, and their apoptosis rates were much lower than that of PBS or siNGF@PBAE. Meanwhile, it is noteworthy that the anti-apoptotic effect of AuDPNAs + L was superior to that of all other groups. Apoptosis is regulated by multiple signaling pathways, which is a process of programmed cell death mediated by caspases. Caspase-3, along with its activated isoform, cleaved caspase-3, modulates apoptosis *via* interactions with various protein factors and is commonly employed as important executors for cellular apoptosis. Solid evidence revealed that caspases can be activated by B cell lymphoma-2 (Bcl-2) family members, such as Bcl-2-associated X (Bax), or inhibited by other members of this family (such as Bcl-2)[62]. In addition, thermal-related HSP-70 protein also plays an important role in protecting chondrocytes[41]. Based on these findings, the apoptosis-related protein (Bcl-2, Bax, caspase-3, and cleaved caspase-3) and HSP-70 in chondrocytes were assessed by western blotting. As shown in Fig. 3E and Supporting Information Fig. S13, treatment by IL-1β induced significant downregulation of Bcl-2 expression while led to the upregulation of the expression of Bax and caspase-3/cleaved caspase-3 proteins, which were obviously alleviated by DIA, AuDs, AuDPNs or AuDPNAs + L. As compared with other groups, AuDPNAs + L treatment elicited more significant alterations in the protein level of Bcl-2, Bax, and caspase-3/cleaved caspase-3 (Fig. 3E and Fig. S13). It is also noteworthy that only AuDPNAs + L significantly increased the expression of HSP-70 in IL-1β-treated chondrocytes (Fig. S13). These results confirmed that AuDPNAs + L reduced chondrocyte apoptosis through the combinational effect of DIA and PTT. To investigate the inflammatory status within chondrocytes, the mRNA levels of tumor necrosis factor (TNF)-α and IL-6[1,3,6] were determined by RT-qPCR. As shown in Supporting Information Fig. S14, IL-1β successfully activated the expression of TNF-α and IL-6 in chondrocytes, and the elevation was repressed after treatment with DIA or nanoparticles containing DIA (AuDs and AuDPNs). The group without DIA, however, could not inhibit the level of TNF-α and IL-6. After the laser irradiation, AuDPNAs also effectively mitigated the IL-1β-induced inflammatory response, suggesting its inhibitory effects.

In cartilage tissue degeneration, the production rate of the matrix from chondrocytes is lower than the hydrolysis rate. The matrix production depends on the function of chondrocytes, and the expression levels of its main components, collagen II (COL2A1) and aggrecan (ACAN), determine the degree of cartilage degeneration to some extent[55]. Moreover, the hydrolysis rate of the matrix depends on the content of various hydrolases, such as TNF) and matrix metalloproteinase 13 (MMP13) that serve as the most potent proteolytic enzymes responsible for the degradation of COL2A1 and ACAN[63-65]. Therefore, the above-mentioned matrix-related protein level is used to evaluate the therapeutic effect of OA treatment. After the pretreatment with IL-1β, the western blotting and RT-qPCR studies revealed that the expression of COL2A1 and ACAN exhibited obvious reduction, whereas the expression of MMP-13 and ADAMTS-5 substantially increased in chondrocytes (Fig. 3F, Supporting Information Figs. S15 and S16). As expected, AuDPNAs + L treatment reversed the IL-1β-induced downregulation of COL2A1 and ACAN. In contrast, the protein expression levels of MMP-13 and ADAMTS-5 greatly decreased after the treatment of AuDPNAs + L. No significant difference was found between IL-1β and siNGF@PBAE, indicating that the addition of siNGF@PBAE did not interfere with the function of chondrocytes. Additionally, we also performed immunofluorescence staining to examine the protein expression level of COL2A1, ACAN, MMP-13, and ADAMTS-5 in chondrocytes. Obviously, the staining intensity of COL2A1 and ACAN was clearly visible, while MMP-13 and ADAMTS-5 decreased significantly after the treatment by AuDPNAs + L (Fig. 3G−J and Supporting Information Fig. S17). The results collectively showed that AuDPNAs could effectively protect the chondrocytes from degradation by downregulating the catabolic proteases (MMP-13, ADAMTS-5) and up-regulating the anabolic components (COL2A1, ACAN).

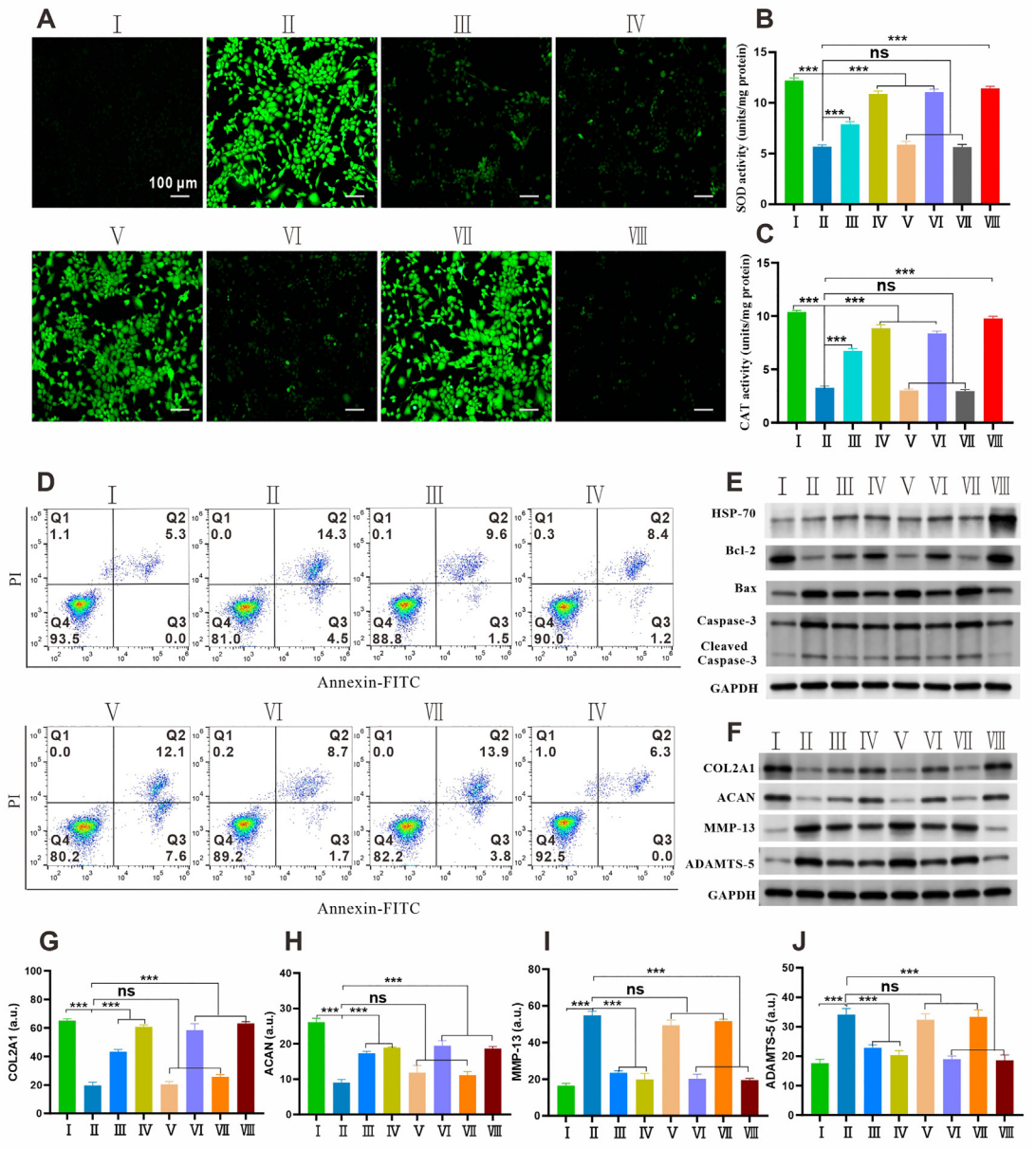

Figure 3 *In vitro* protective effects of the nanodrug on chondrocytes against ROS and apoptosis. IL-1β (10 ng/mL) was applied in chondrocytes to mimic the pathological process of OA, and was co-cutreated with PBS (II), DIA (III), AuDs (IV), siNGF@PBAE (V), AuDPNs (VI), AuDPNAs (VII), and AuDPNAs + L (VIII), along with a blank control group (I). (A) Intracellular ROS levels were assessed in chondrocytes using DCFH-DA. Scale bar: 100 μm. (B) SOD activity assay of chondrocytes (n = 3). (C) CAT activity assay of chondrocytes (n = 3). (D) Chondrocytes apoptosis was assessed by flow cytometry after labeling with annexin V−fluorescein isothiocyanate (FITC) conjugate and propidium iodide (PI) (n = 4). (E) The Western blot analysis of chondrocytes, showed the protein expression of HSP-70, Bax, Bcl-2, caspase-3, and cleaved caspase-3 (n = 3). (F) The protein expression of COL2A1, ACAN, MMP-13, and ADAMTS-5 expression in chondrocytes (n = 3). (G−J) Quantitation of COL2A1 (G), ACAN (H), MMP-13 (I), and ADAMTS-5 (J) expression in chondrocytes tested by immunofluorescent staining (n = 3). Data are presented as mean ± S.D. Significance was calculated using one-way ANOVA with Tukey's *post hoc* test. ***$P < 0.001$. ns, no significant difference.

3.5. *In vivo photothermal responsiveness and drug release behavior*

IA injection is recognized as an effective administration route for OA treatment. However, the drug administered into synovial joint is rapidly eliminated across the synovial membrane, and distribution into cartilage is limited, resulting in unsatisfactory therapeutic outcomes[16]. Therefore, the *in vivo* retention and the photothermal release behavior of our system were evaluated. By photothermal imaging, we observed that there were no obvious temperature changes after saline treatment, while elevated temperature was detected after either AuNCs or AuDPNAs treatment (Fig. 4A). We also found that there were no obvious differences in temperature between AuDPNAs and AuNCs after 5 min

irradiation, suggesting that the coating of LA/SA and PBAE could not influence the thermal properties of AuNCs (Fig. 4B).

We used a fluorescence dye, cyanine 5 (Cy5), as the model drug of DIA to investigate the drug distribution. Cy5 was loaded into AuNCs to produce Cy5-loaded AuNCs nanoparticles, including AuDs, AuDPNAs, and AuDPNAs + L. As depicted in Fig. 4C, a strong fluorescence signal was observed in all groups during the initial 7 days. However, on Day 14, the fluorescence signals in Cy5 and AuDs groups gradually diminished, becoming nearly undetectable after 28 days of treatment. In contrast, the visible fluorescence signal was detected after the treatment by AuDPNAs or AuDPNAs + L at the treatment for 28 days. Furthermore, the quantitative analysis of the total radiant efficiency data within the anatomical region of interest (ROI) over 28 days of treatment indicated that AuDPNAs significantly increased the retention of model drugs in the synovial joint (Fig. 4D). All these results indicated that the cationic PBAE contributes to prolonged drug retention, whereas the coating of LA/SA effectively facilitates drug release. These results indicate that utilizing LA/SA not only enhances the local retention capability of AuDPNs upon injection but also continuously reduces the loss of DIA within the synovial joint, enabling DIA to exert its effects as needed for an extended period after a single injection.

3.6. *In vivo therapeutic effect of joint degeneration on OA mice model*

We further proceeded to evaluate the *in vivo* therapeutic efficacy of our system using an OA mouse model *via* intra-articular (IA) injection. To this end, we employed destabilization of the medial meniscus (DMM) surgery in C57 mice to establish the OA model (Fig. 5A). Subsequently, the mice were divided into five groups (G2-G5: DMM + PBS, DMM + DIA, DMM + siNGF@PBAE, DMM + AuDPNAs, DMM + AuDPNAs + L), with G1 serving as

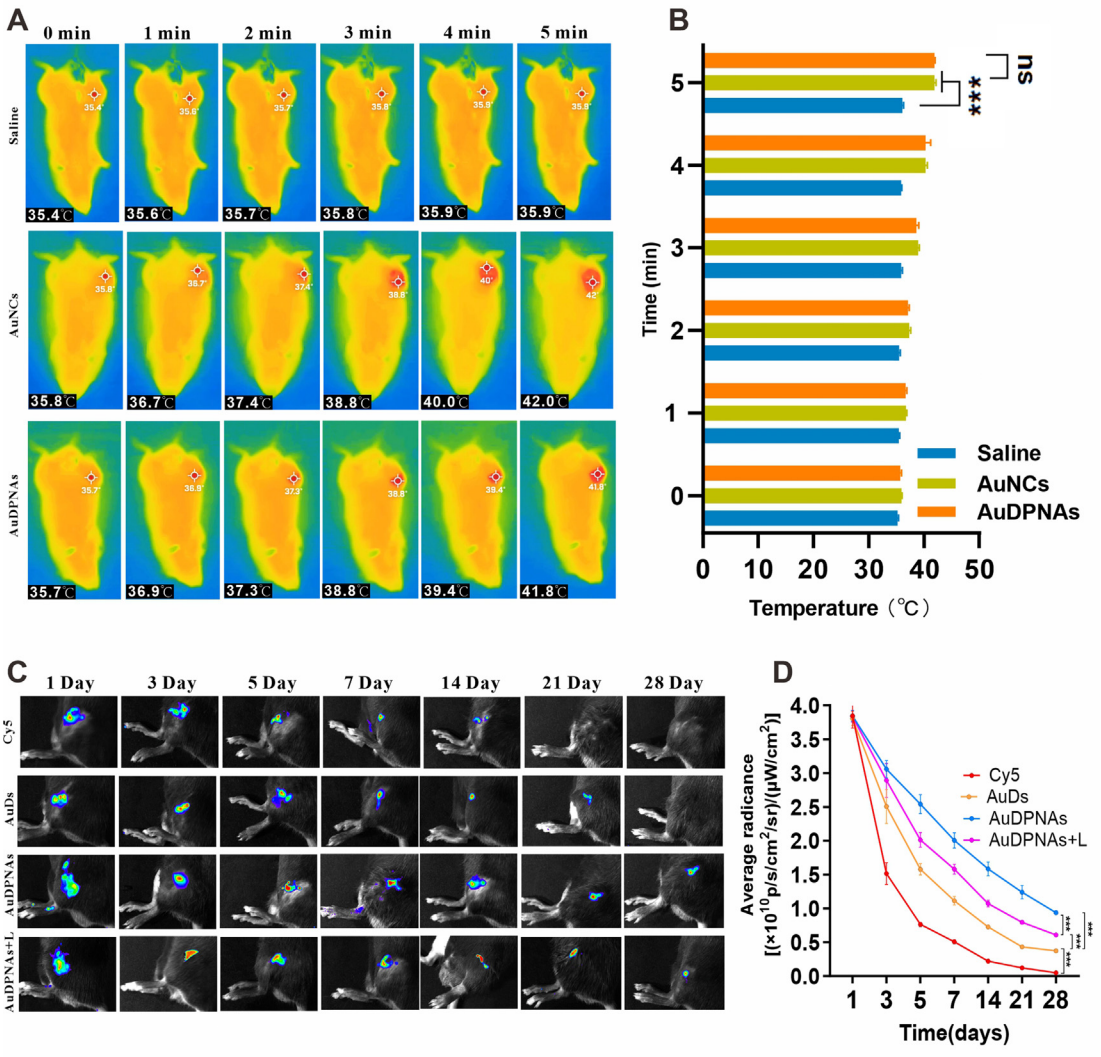

Figure 4 Intra-articular residence and photothermal conversion property of nanodrug. (A) The photothermal performance of AuNCs and AuDPNAs in knee joints upon laser irradiation (808 nm, 0.2 W/cm^2) over 5 min ($n = 5$). (B) *In vivo* joint temperature variations with and without AuNCs at specific intervals ($n = 5$). (C) IVIS images displaying mice knee joints across 28 days post-injection with Cy5, AuDs, AuDPNAs, and AuDPNAs + L ($n = 5$). (D) Temporal progression of fluorescent radiant efficiency within the joints at indicated time points ($n = 5$). Data are presented as mean ± S.D. Significance was calculated using two-way ANOVA with Bonferroni *post-hoc* test. $^{**}P < 0.01$, $^{***}P < 0.001$, ns, no significant difference.

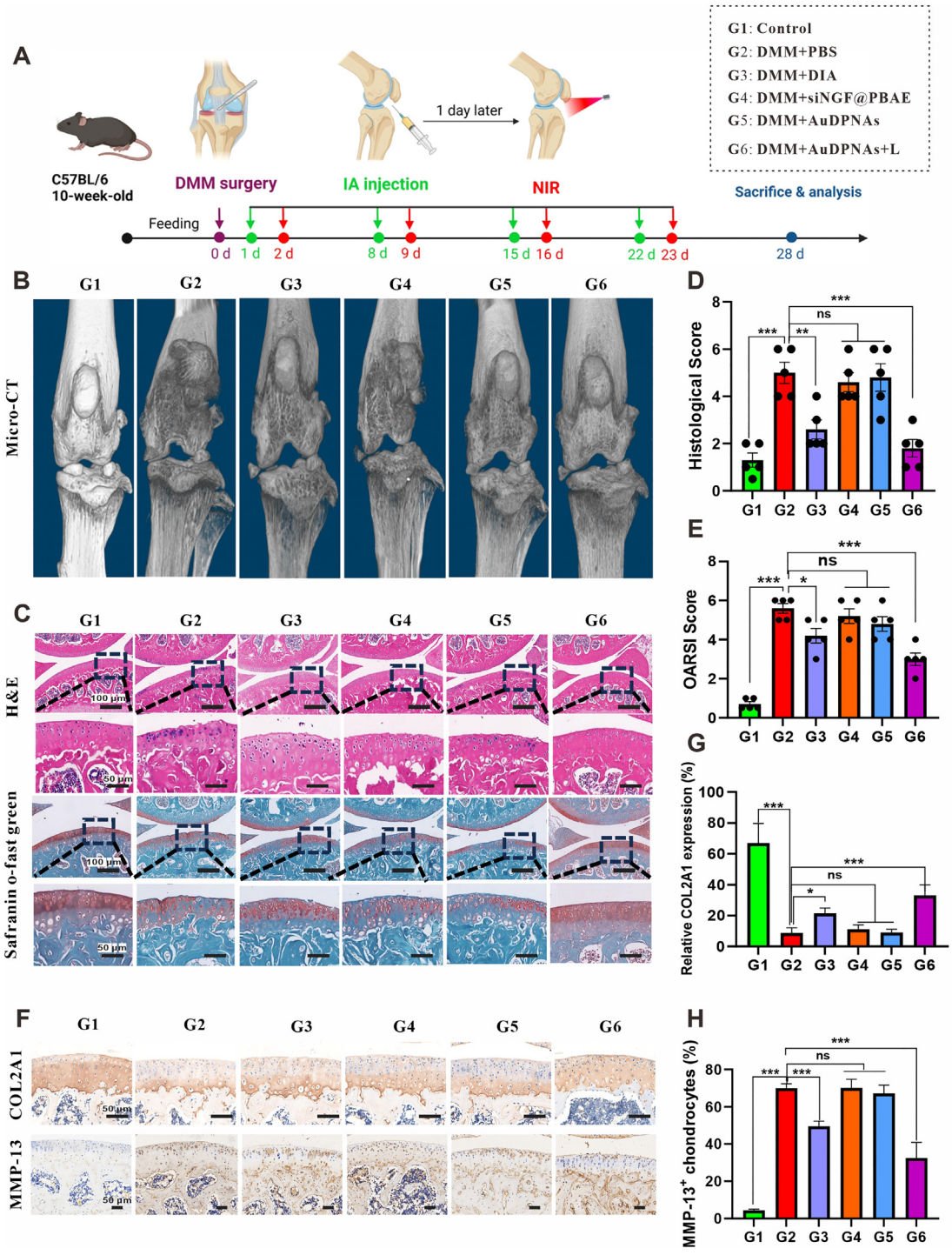

Figure 5 The nanodrug under laser irradiation exhibited cartilage protection in mice. (A) Regimen illustration for the DMM-induced OA model. (B) Exemplary micro-CT scans of each group ($n = 5$). (C) Histological staining analysis was conducted on the cartilage sections using the H&E and Safranin O-Fast Green methods to evaluate the treatment of DMM-induced OA mice after being injected with PBS (G2), DIA (G3), siNGF@PBAE (G4), AuDPNAs (G5), and AuDPNAs + L (G6) at 4 weeks post-surgery ($n = 5$). Scale bar: 50, 100 μm. (D, E) Histological (D) and OARSI (E) scores of the articular cartilage for each group were assessed after the 4-week treatment period ($n = 5$). (F) Representative fluorescence images displaying the expression of COL2A1 and MMP-13 proteins in the articular cartilage, 4 weeks post intra-articular injection of G2−G6 ($n = 5$). Scale bar: 50 μm. (G, H) COL2A1 protein expression level (G) and percentage of MMP-13-positive chondrocytes (H) obtained from the fluorescence intensity ($n = 5$). Data are presented as mean ± S.D. Significance was calculated using one-way ANOVA with Tukey's *post-hoc* test. $^{*}P < 0.05$, $^{**}P < 0.01$, $^{***}P < 0.001$. ns, no significant difference.

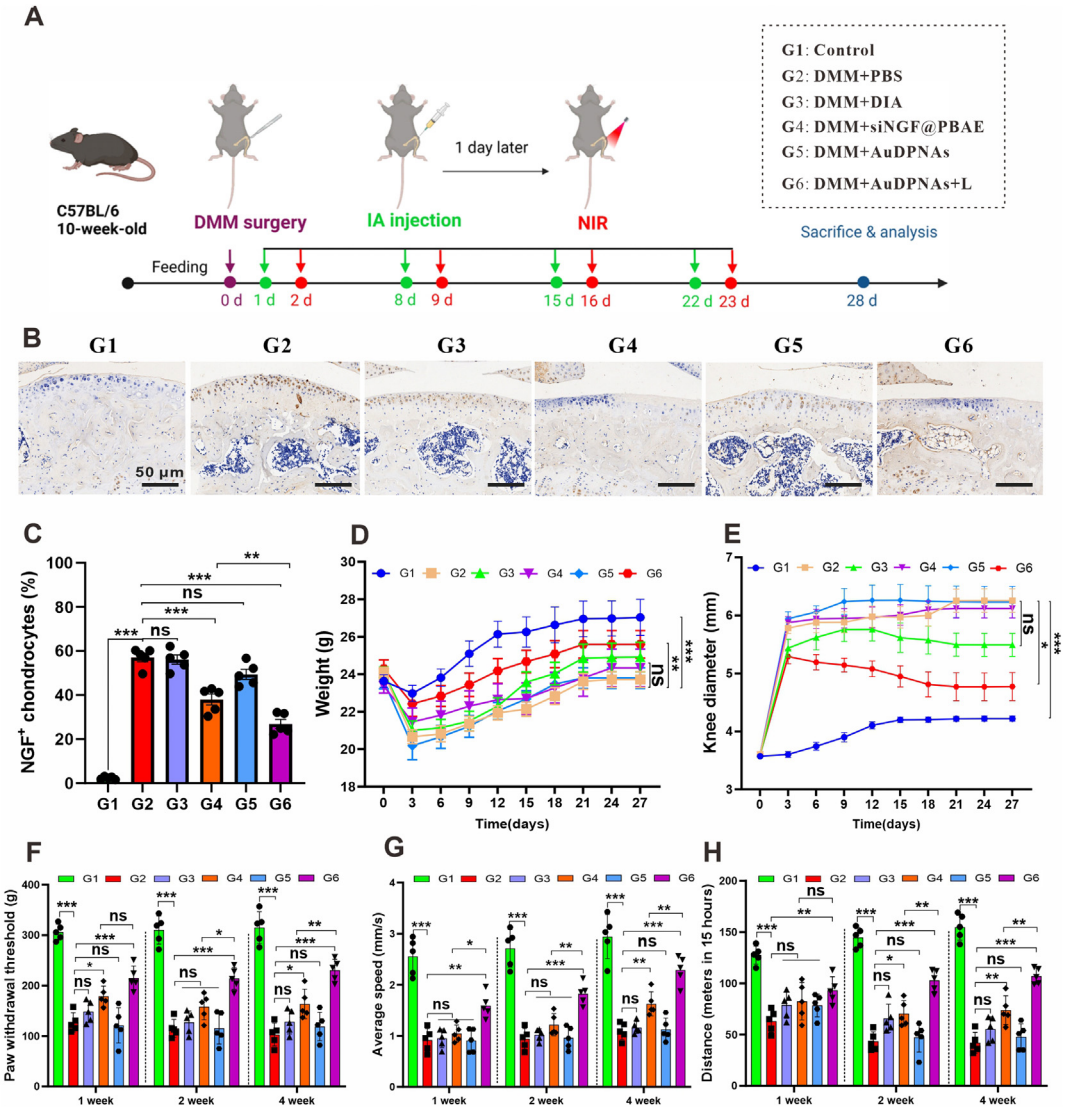

Figure 6 *In vivo* NGF knockdown and modulation of pain-related symptoms with nanodrug in OA model. (A) Illustration of the mitigation process of DMM-induced OA pain-related behaviors. (B) Representative fluorescent images of NGF protein expression levels in articular cartilage following intra-articular injection of PBS (G2), DIA (G3), siNGF@PBAE (G4), AuDPNAs (G5), and AuDPNAs + L (G6) into the knee joints of mice at 4 weeks postoperatively ($n = 5$ biologically independent mice). Scale bar: 50 μm. (C) Assessment of NGF-positive cells proportion in cartilage ($n = 5$ biologically independent mice). (D, E) The weight (D) and diameter (E) of mice were measured at 3-day intervals until their sacrifice ($n = 5$ biologically independent mice). (F−H) Assessment of pain sensitivity and mobility by paw withdrawal threshold (F), average speed (G) and distance (H) test at 1, 2, and 4 weeks post-surgery ($n = 5$ biologically independent mice). Data are presented as mean ± S.D. Significance was calculated using one-way ANOVA with Tukey's *post-hoc* test (C, F−H) or two-way ANOVA with Bonferroni *post-hoc* test (D and E). $^{*}P < 0.05$, $^{**}P < 0.01$, $^{***}P < 0.001$, ns, no significant difference.

a negative control from normal mice. 4 weeks post-DMM surgery, the PBS treatment (G2) displayed significant joint degeneration and cartilage injury, confirming the successful establishment of OA model (Fig. 5B). Thus, the model mice were subjected to IA injection into the joint once every 7 days for consecutive 3 weeks before therapy evaluation (Fig. 5A). As depicted in Fig. 5B, the representative micro-CT images revealed that the articular surface of G2−G4 exhibited destruction with numerous osteophytes, indicative of severe joint degeneration following treatment with DIA alone or siRNA alone. AuDPNAs treatment without laser stimulation (G5) displayed moderate therapeutic effects. However, the treatment by AuDPNAs + L (G6) demonstrated significant improvement in joint degeneration, with no obvious difference compared to the control group G1 (healthy mice). This direct evidence underscores the substantial therapeutic effect of AuDPNAs + L in mitigating the progression of OA.

To further substantiate the favorable anti-osteoarthritis (OA) treatment effects of our nanodrug, we conducted various immunohistochemical analyses, including hematoxylin−eosin (H&E) staining, safranin O-fast green staining, and alcian blue-hematoxylin/orange G (ABH/OG), to histologically evaluate the cartilage tissues. In Fig. 5C, the typical OA features, such as vertical fissure, erosion denudation, surface discontinuity, and deformation, were evident in G2. Regarding matrix staining, morphological changes, and tidemark integrity promotion, G3 and G6 demonstrated a certain degree of improvement as compared to G2, while

the therapeutic effects in G4 and G5 were less evident. Notably, G6 treatment exhibited the most significant preservation of the columnar architecture of normal cartilage, manifested by decreased surface denudation and deformation, increased tissue cellularity and cloning, and less severe lesions and extensive erosion. Moreover, the safranin ABH-positive staining was observed to be much stronger after G6 treatment, as compared with other treatments (G2−G5) (Supporting Information Fig. S18). To quantitatively assess the degree of cartilage damage, Osteoarthritis Research Society International (OARSI) and histological scores[55-57] of all groups were determined. As illustrated in Fig. 5D, the histological score of cartilage indicated that G6 exhibited superior performance in mitigating cartilage matrix depletion and maintaining overall cartilage thickness. Similarly, compared to the G2 group, all other treatment groups showed varying degrees of reduction in their OARSI scores. Notably, the G6 group exhibited the most significant improvement, with OARSI scores decreasing by approximately 54% (Fig. 5E). Furthermore, the immunohistochemistry staining was performed to detect the protein expression levels of COL2A1 and MMP-13 in chondrocytes of the cartilage tissues (Fig. 5F). Four weeks after DMM surgery, the COL2A1 protein expression level significantly decreased, with the staining intensity of G1 visibly higher than that of G2. Conversely, the expression trend of MMP-13 was opposite to that of COL2A1. G6 significantly increased the COL2A1 and simultaneously decreased MMP-13 protein expression levels compared to other groups (Fig. 5G and H). These comprehensive histological analyses provide robust evidence to support the significant therapeutic efficacy of AuDPNAs + L in OA treatment.

3.7. In vivo modulation of pain-related behavior in OA mice model

Pain relief is a crucial criterion for the evaluation of anti-osteoarthritis (OA) drugs[18]. Therefore, the pain-related evaluations of different groups (G1: Control, G2-G6: DMM + PBS, DMM + DIA, DMM + siNGF@PBAE, DMM + AuDPNAs, DMM + AuDPNAs + L) were investigated in the OA mouse model (Fig. 6A). As depicted in Fig. 6B and C, the immunohistochemical staining showed that DMM surgery (G2) induced increased NGF overexpression in the cartilage matrix, and NGF overexpression was suppressed following G4 and G6 treatment. Additionally, body weight and knee diameter were recorded at the end of the treatment (Day 28). Fig. 6D illustrated that all mice in G6 group maintained sustained and steady growth of body weight, while a significant decrease was observed in G2 group. Compared with G1, DMM surgery increased the knee joint diameter significantly during the initial 3 days in G6, which was recovered to near-normal levels after G6 treatment (Fig. 6E). Moreover, the OA pain sensitivity of G1−G6 was determined by pressure application measurement (PAM) device at 1, 2, and 4 weeks after DMM surgery. In Fig. 6F, the mice in G2 group exhibited significant reduction in paw withdrawal response thresholds, while G6 treatment significantly increased the paw withdrawal response threshold, indicating reduced pain sensitivity. In contrast, the slight effect on reversing the paw withdrawal response threshold and reducing pain sensitivity was observed in G4 group. This effect can be attributed to the reduction of inflammation, swelling, pain relief, and improvement of blood circulation through thermal therapy[40]. In addition to pain relief, the improvement in the motility of OA mice after treatment was observed. The tests of average speed (cm/s) and distance (cm in 15 h) showed that healthy mice could stay on the test bench for a longer duration compared to OA mice. After irradiation, the walking performance of the mice in G6 group improved significantly compared to the G4 group, while G3 and G5 groups had no significant effects (Fig. 6G and H). These results collectively suggested that our therapeutic system achieved satisfactory pain relief and greatly improved motor function in a well-received DMM OA model.

4. Conclusions

In summary, we developed the AuNCs-based nanodrug, which could effectively co-deliver the anti-inflammatory drug DIA and pain-relieving siNGF, for the treatment of OA. Beyond the anti-inflammatory properties of DIA, our AuNCs-based nanodrug demonstrated a high transfection efficiency of siRNA through the modification of cationic PBAE in chondrocytes, as well as improved the expression of HSP70, fortifying the protection of chondrocytes through the photothermal effect generated by AuNCs. The coating of LA/SA layer rendered the thermo-responsiveness to modulate DIA drug release through photothermal effect. After IA injection, the nanodrug system significantly increased the retention of model drugs in the synovial joint. In the OA mouse model, the combinational effects of our nanodrug not only protected chondrocytes from degeneration and alleviated OA-induced pain, but also inhibited the progression of OA. These findings provide promising avenues for the development of a straightforward, convergent, and effective strategy to improve the treatment of OA.

However, despite these promising results, the synthesis of such complex nanodrugs may present challenges in cost and scalability for widespread clinical use. Concerns about the long-term effects of nanoparticles and the requirement for external light for drug release modulation could limit its practical applications and pose regulatory hurdles. Furthermore, extensive evaluations to ensure safety and efficacy are still essential before its clinical practice for patients.

Acknowledgments

The authors acknowledge the National Natural Science Foundation of China (82172458, 82371589, 82073779, and 32000992) and Natural Science Foundation of Zhejiang Province (Distinguished Young Scholar Program, No. LR21H300002, China).

Author contributions

Li Qiao: Writing − original draft, Methodology, Investigation, Formal analysis, Data curation. Zhiyao Li: Methodology, Investigation, Conceptualization. Bowen Li: Writing − review & editing, Writing − original draft, Methodology, Conceptualization. Fu Zhang: Methodology, Investigation. Zhuo Yao: Methodology. Chongzhi Wu: Investigation. Honglin Tang: Methodology, Investigation. Qi Pan: Methodology. Peihua Shi: Writing − review & editing, Writing − original draft, Supervision, Project administration, Conceptualization. Yuan Ping: Writing − review & editing, Writing − original draft, Supervision, Project administration, Conceptualization.

Conflicts of interest

The authors have no conflicts of interest to declare.

Appendix A. Supporting information

Supporting information to this article can be found online at https://doi.org/10.1016/j.apsb.2024.06.009.

References

1. Hunter DJ, Bierma-Zeinstra S. Osteoarthritis. *Lancet* 2019;**393**:1745−59.
2. Cui A, Li H, Wang D, Zhong J, Chen Y, Lu H. Global, regional prevalence, incidence and risk factors of knee osteoarthritis in population-based studies. *EClinicalMedicine* 2020;**29**−**30**:100587.
3. Mobasheri A, Rayman MP, Gualillo O, Sellam J, van der Kraan P, Fearon U. The role of metabolism in the pathogenesis of osteoarthritis. *Nat Rev Rheumatol* 2017;**13**:302−11.
4. Zhang Y, Su D, Wang Y, Wang Z, Ren Y, Liu R, et al. Locally delivered modified citrus pectin — a galectin-3 inhibitor shows expected anti-inflammatory and unexpected regeneration-promoting effects on repair of articular cartilage defect. *Biomaterials* 2022;**291**:121870.
5. Karsdal MA, Michaelis M, Ladel C, Siebuhr AS, Bihlet AR, Andersen JR, et al. Disease-modifying treatments for osteoarthritis (DMOADs) of the knee and hip: lessons learned from failures and opportunities for the future. *Osteoarthritis Cartilage* 2016;**24**:2013−21.
6. Chen D, Shen J, Zhao W, Wang T, Han L, Hamilton JL, et al. Osteoarthritis: toward a comprehensive understanding of pathological mechanism. *Bone Res* 2017;**5**:16044.
7. Yudoh K, Nguyen v T, Nakamura H, Hongo-Masuko K, Kato T, Nishioka K. Potential involvement of oxidative stress in cartilage senescence and development of osteoarthritis: oxidative stress induces chondrocyte telomere instability and downregulation of chondrocyte function. *Arthritis Res Ther* 2005;**7**:R380−91.
8. Zheng L, Zhang Z, Sheng P, Mobasheri A. The role of metabolism in chondrocyte dysfunction and the progression of osteoarthritis. *Ageing Res Rev* 2021;**66**:101249.
9. Li J, Han F, Ma J, Wang H, Pan J, Yang G, et al. Targeting endogenous hydrogen peroxide at bone defects promotes bone repair. *Adv Funct Mater* 2022;**32**:2111208.
10. Lepetsos P, Papavassiliou KA, Papavassiliou AG. Redox and NF-κB signaling in osteoarthritis. *Free Radic Biol Med* 2019;**132**:90−100.
11. Martel-Pelletier J, Pelletier JP. Effects of diacerein at the molecular level in the osteoarthritis disease process. *Ther Adv Musculoskelet Dis* 2010;**2**:95−104.
12. Almezgagi M, Zhang Y, Hezam K, Shamsan E, Gamah M, Al-Shaebi F, et al. Diacerein: recent insight into pharmacological activities and molecular pathways. *Biomed Pharmacother* 2020;**131**:110594.
13. Chen X, Zhu X, Dong J, Chen F, Gao Q, Zhang L, et al. Reversal of epigenetic peroxisome proliferator-activated receptor-γ suppression by diacerein alleviates oxidative stress and osteoarthritis in mice. *Antioxid Redox Sign* 2022;**37**:40−53.
14. Pavelka K, Bruyère O, Cooper C, Kanis JA, Leeb BF, Maheu E, et al. Diacerein: benefits, risks and place in the management of osteoarthritis. An opinion-based report from the ESCEO. *Drugs Aging* 2016;**33**:75−85.
15. Jain A, Singh SK, Singh Y, Singh S. Development of lipid nanoparticles of diacerein, an antiosteoarthritic drug for enhancement in bioavailability and reduction in its side effects. *J Biomed Nanotechnol* 2013;**9**:891−900.
16. Maudens P, Jordan O, Allémann E. Recent advances in intra-articular drug delivery systems for osteoarthritis therapy. *Drug Discov Today* 2018;**23**:1761−75.
17. Zhao T, Li X, Li H, Deng H, Li J, Yang Z, et al. Advancing drug delivery to articular cartilage: from single to multiple strategies. *Acta Pharm Sin B* 2023;**13**:4127−48.
18. Jung JH, Kim SE, Kim HJ, Park K, Song GG, Choi SJ. A comparative pilot study of oral diacerein and locally treated diacerein-loaded nanoparticles in a model of osteoarthritis. *Int J Pharmacol* 2020;**581**:119249.
19. Serge P, Anne-Priscille T. Pain in osteoarthritis from a symptom to a disease. *Best Pract Res Clin Rheumatol* 2023:101825.
20. Dorn G, Patel S, Wotherspoon G, Hemmings-Mieszczak M, Barclay J, Natt FJ, et al. siRNA relieves chronic neuropathic pain. *Nucleic Acids Res* 2004;**32**:e49.
21. Akhilesh, Uniyal A, Gadepalli A, Tiwari V, Allani M, Chouhan D, et al. Unlocking the potential of TRPV1 based siRNA therapeutics for the treatment of chemotherapy-induced neuropathic pain. *Life Sci* 2022;**288**:120187.
22. Denk F, Bennett DL, McMahon SB. Nerve growth factor and pain mechanisms. *Annu Rev Neurosci* 2017;**40**:307−25.
23. Schmelz M, Mantyh P, Malfait AM, Farrar J, Yaksh T, Tive L, et al. Nerve growth factor antibody for the treatment of osteoarthritis pain and chronic low-back pain: mechanism of action in the context of efficacy and safety. *Pain* 2019;**160**:2210−20.
24. Iannone F, De Bari C, Dell'Accio F, Covelli M, Patella V, Lo Bianco G, et al. Increased expression of nerve growth factor (NGF) and high affinity NGF receptor (p140 TrkA) in human osteoarthritic chondrocytes. *Rheumatology* 2002;**41**:1413−8.
25. Driscoll C, Chanalaris A, Knights C, Ismail H, Sacitharan PK, Gentry C, et al. Nociceptive sensitizers are regulated in damaged joint tissues, including articular cartilage, when osteoarthritic mice display pain behavior. *Arthritis Rheumatol* 2016;**68**:857−67.
26. Bishop CJ, Tzeng SY, Green JJ. Degradable polymer-coated gold nanoparticles for co-delivery of DNA and siRNA. *Acta Biomater* 2015;**11**:393−403.
27. Sardo C, Bassi B, Craparo EF, Scialabba C, Cabrini E, Dacarro G, et al. Gold nanostar-polymer hybrids for siRNA delivery: polymer design towards colloidal stability and *in vitro* studies on breast cancer cells. *Int J Pharmacol* 2017;**519**:113−24.
28. Shi P, Liu Z, Dong K, Ju E, Ren J, Du Y, et al. A smart "sense-act-treat" system: combining a ratiometric pH sensor with a near infrared therapeutic gold nanocage. *Adv Mater* 2014;**26**:6635−41.
29. He H, Liu L, Zhang S, Zheng M, Ma A, Chen Z, et al. Smart gold nanocages for mild heat-triggered drug release and breaking chemoresistance. *J Control Release* 2020;**323**:387−97.
30. Hussein EA, Zagho MM, Nasrallah GK, Elzatahry AA. Recent advances in functional nanostructures as cancer photothermal therapy. *Int J Nanomedicine* 2018;**13**:2897−906.
31. Chen Y, Gao Y, Chen Y, Liu L, Mo A, Peng Q. Nanomaterials-based photothermal therapy and its potentials in antibacterial treatment. *J Control Release* 2020 2020;**328**:251−62.
32. Lv Z, He S, Wang Y, Zhu X. Noble metal nanomaterials for NIR-triggered photothermal therapy in cancer. *Adv Healthc Mater* 2021;**10**:e2001806.
33. Tang X, Tan L, Shi K, Peng J, Xiao Y, Li W, et al. Gold nanorods together with HSP inhibitor-VER-155008 micelles for colon cancer mild-temperature photothermal therapy. *Acta Pharm Sin B* 2018;**8**:587−601.
34. Yang W, Liang H, Ma S, Wang D, Huang J. Gold nanoparticle based photothermal therapy: development and application for effective cancer treatment. *Sustain Mater Techno* 2019;**22**:e00109.
35. Shen W, Wang R, Fan Q, Gao X, Wang H, Shen Y, et al. Natural polyphenol inspired polycatechols for efficient siRNA delivery. *CCS Chem* 2020;**2**:146−57.
36. Fan Q, Yang Z, Li Y, Cheng Y, Li Y. Polycatechol mediated small interfering RNA delivery for the treatment of ulcerative colitis. *Adv Funct Mater* 2021;**31**:2101646.
37. Morgan E, Wupperfeld D, Morales D, Reich N. Shape matters: gold nanoparticle shape impacts the biological activity of siRNA delivery. *Bioconjug Chem* 2019;**30**:853−60.
38. Xia Y, Li W, Cobley CM, Chen J, Xia X, Zhang Q, et al. Gold nanocages: from synthesis to theranostic applications. *Acc Chem Res* 2011;**44**:914−24.
39. Pang B, Yang X, Xia Y. Putting gold nanocages to work for optical imaging, controlled release and cancer theranostics. *Nanomedicine* 2016;**11**:1715−28.

40. Li L, Zhang X, Zhou J, Zhang L, Xue J, Tao W. Non-invasive thermal therapy for tissue engineering and regenerative medicine. *Small* 2022; **18**:e2107705.
41. Lin F, Zhuang Y, Xiang L, Ye T, Wang Z, Wu L, et al. Localization of lesion cells and targeted mitochondria *via* embedded hydrogel microsphere using heat transfer microneedles. *Adv Funct Mater* 2023; **33**:2212730.
42. Li X, Dai B, Guo J, Zheng L, Guo Q, Peng J, et al. Nanoparticle-cartilage interaction: pathology-based intra-articular drug delivery for osteoarthritis therapy. *Nano-micro Lett* 2021;**13**:149.
43. Lin F, Wang Z, Xiang L, Deng L, Cui W. Charge-guided micro/nano-hydrogel microsphere for penetrating cartilage matrix. *Adv Funct Mater* 2021;**31**:2107678.
44. Chen L, Zhang J, Wang J, Lin J, Luo X, Cui W. Inflammation-regulated auto aggregated hydrogel microspheres *via* anchoring cartilage deep matrix for genes delivery. *Adv Funct Mater* 2023; **33**:2305635.
45. Karlsson J, Rhodes KR, Green JJ, Tzeng SY. Poly(beta-amino ester)s as gene delivery vehicles: challenges and opportunities. *Expert Opin Drug Deliv* 2020;**17**:1395−410.
46. Yan X, Pan Q, Xin H, Chen Y, Ping Y. Genome-editing prodrug: targeted delivery and conditional stabilization of CRISPR-Cas9 for precision therapy of inflammatory disease. *Sci Adv* 2021;**7**: eabj0624.
47. Zhu C, Huo D, Chen Q, Xue J, Shen S, Xia Y. A eutectic mixture of natural fatty acids can serve as the gating material for near-infrared-triggered drug release. *Adv Mater* 2017;**29**:10.1002/adma.201703702.
48. Perni S, Prokopovich P. Poly-beta-amino-esters nano-vehicles based drug delivery system for cartilage. *Nanomed Nanotechnol Biol Med* 2017;**13**:539−48.
49. Perni S, Prokopovich P. Optimisation and feature selection of poly-beta-amino-ester as a drug delivery system for cartilage. *J Mater Chem B* 2020;**8**:5096−108.
50. Saeedi T, Prokopovich P. Poly beta amino ester coated emulsions of NSAIDs for cartilage treatment. *J Mater Chem B* 2021;**9**:5837−47.
51. Chen Y, Chen X, Wu D, Xin H, Chen D, Li D, et al. Delivery of CRISPR/Cas9 plasmids by cationic gold nanorods: impact of the aspect ratio on genome editing and treatment of hepatic fibrosis. *Chem Mater* 2021;**33**:81−91.
52. Chen X, Chen Y, Xin H, Wan T, Ping Y. Near-infrared optogenetic engineering of photothermal nanoCRISPR for programmable genome editing. *Proc Natl Acad Sci USA* 2020;**117**:2395−405.
53. Tang H, Xu X, Chen Y, Xin H, Wan T, Li B, et al. Reprogramming the tumor microenvironment through second-near-infrared-window photothermal genome editing of PD-L1 mediated by supramolecular gold nanorods for enhanced cancer immunotherapy. *Adv Mater* 2021;**33**: e2006003.
54. Chen J, Yang M, Zhang Q, Cho EC, Cobley CM, Kim C, et al. Gold nanocages: a novel class of multifunctional nanomaterials for theranostic applications. *Adv Funct Mater* 2010;**20**:3684−94.
55. Wang W, Duan J, Ma W, Xia B, Liu F, Kong Y, et al. Trimanganese tetroxide nanozyme protects cartilage against degeneration by reducing oxidative stress in osteoarthritis. *Adv Sci* 2023;**10**: e2205859.
56. Pritzker KP, Gay S, Jimenez SA, Ostergaard K, Pelletier JP, Revell PA, et al. Osteoarthritis cartilage histopathology: grading and staging. *Osteoarthritis Cartilage* 2006;**14**:13−29.
57. Glasson SS, Chambers MG, Van Den Berg WB, Little CB. The OARSI histopathology initiative—recommendations for histological assessments of osteoarthritis in the mouse. *Osteoarthritis Cartilage* 2010;**18**(Suppl 3):S17−23.
58. Pecchi E, Priam S, Gosset M, Pigenet A, Sudre L, Laiguillon MC, et al. Induction of nerve growth factor expression and release by mechanical and inflammatory stimuli in chondrocytes: possible involvement in osteoarthritis pain. *Arthritis Res Ther* 2014;**16**:R16.
59. Hui W, Young DA, Rowan AD, Xu X, Cawston TE, Proctor CJ. Oxidative changes and signalling pathways are pivotal in initiating age-related changes in articular cartilage. *Ann Rheum Dis* 2016;**75**:449−58.
60. Afonso V, Champy R, Mitrovic D, Collin P, Lomri A. Reactive oxygen species and superoxide dismutases: role in joint diseases. *Jt Bone Spine* 2007;**74**:324−9.
61. Hwang HS, Kim HA. Chondrocyte apoptosis in the pathogenesis of osteoarthritis. *Int J Mol Sci* 2015;**16**:26035−54.
62. Ling Q, Xu X, Wei X, Wang W, Zhou B, Wang B, et al. Oxymatrine induces human pancreatic cancer PANC-1 cells apoptosis *via* regulating expression of Bcl-2 and IAP families, and releasing of cytochrome c. *J Exp Clin Cancer Res* 2011;**30**:66.
63. Hu Q, Ecker M. Overview of MMP-13 as a Promising target for the treatment of osteoarthritis. *Int J Mol Sci* 2021;**22**:1742.
64. Latourte A, Richette P. Inhibition of ADAMTS-5: the right target for osteoarthritis?. *Osteoarthritis Cartilage* 2022;**30**:175−7.
65. Verma P, Dalal K. ADAMTS-4 and ADAMTS-5: key enzymes in osteoarthritis. *J Cel Biochem* 2011;**112**:3507−14.